NASA TM X-813

TECHNICAL MEMORANDUM

X-813

EXPERIMENTAL INVESTIGATION OF THE OVERALL PRESSURE DISTRIBUTION, FLOW FIELD, AND AFTERBODY HEAT-TRANSFER DISTRIBUTION OF AN APOLLO REENTRY CONFIGURATION AT A MACH NUMBER OF 8

By Robert A. Jones

Langley Research Center
Langley Station, Hampton, Va.

NATIONAL AERONAUTICS AND SPACE ADMINISTRATION
WASHINGTON

June 1963

Cycle 2

ERRATA

NASA Technical Memorandum X-813

EXPERIMENTAL INVESTIGATION OF THE OVERALL PRESSURE DISTRIBUTION, FLOW FIELD, AND AFTERBODY HEAT-TRANSFER DISTRIBUTION OF AN APOLLO REENTRY CONFIGURATION AT A MACH NUMBER OF 8

By Robert A. Jones

June 1963

The values computed for the stagnation-point velocity gradients on page 6 are in error, and the following corrections should be made:

Page 6, line 26:

$$\left(\frac{d\,\frac{V}{V_\infty}}{d\,\frac{s}{r_n}}\right)_{\frac{s}{r_n}=0} = 0.744$$

Page 6, line 30:

$$\left(\frac{d\,\frac{V}{V_\infty}}{d\,\frac{s}{r_n}}\right)_{\frac{s}{r_n}=0} = 0.656$$

Page 6, line 33: The quantity 0.23 should be 0.552.

NASA-Langley, 1963

Issued 11-8-63

X63-13304

ERRATA

NASA Technical Memorandum X-813

EXPERIMENTAL INVESTIGATION OF THE OVERALL PRESSURE DISTRIBUTION, FLOW FIELD, AND AFTERBODY HEAT-TRANSFER DISTRIBUTION OF AN APOLLO REENTRY CONFIGURATION AT A MACH NUMBER OF 8

By Robert A. Jones
June 1963

The values computed for the stagnation-point velocity gradients on page 6 are in error, and the following corrections should be made:

Page 6, line 26:

$$\left(\frac{d\,\frac{V}{V_\infty}}{d\,\frac{s}{r_n}}\right)_{\frac{s}{r_n}=0} = 0.744$$

Page 6, line 30:

$$\left(\frac{d\,\frac{V}{V_\infty}}{d\,\frac{s}{r_n}}\right)_{\frac{s}{r_n}=0} = 0.656$$

Page 6, line 33: The quantity 0.23 should be 0.552.

NASA-Langley, 1963

Issued 11-8-63

NATIONAL AERONAUTICS AND SPACE ADMINISTRATION

TECHNICAL MEMORANDUM X-813

EXPERIMENTAL INVESTIGATION OF THE OVERALL PRESSURE DISTRIBUTION, FLOW FIELD, AND AFTERBODY HEAT-TRANSFER DISTRIBUTION OF AN APOLLO REENTRY CONFIGURATION AT A MACH NUMBER OF 8* **

By Robert A. Jones

SUMMARY

Measured heat-transfer and pressure distributions on the afterbody of an Apollo reentry configuration, the pressure distribution along the vertical plane of symmetry of the face, schlieren studies, oil-flow patterns, and wake surveys were obtained in a conventional Mach number 8 tunnel. The angle of attack was varied from 0° to 55°. The Reynolds number based on face diameter and free-stream properties ranged from 0.10×10^6 to 1.36×10^6.

The flow over the body was laminar and it separated just downstream of the point where the body surface became parallel to the free stream. The angle between the free stream and the tangent to the surface at this point was about 10° and was independent of angle of attack. In this separated region the pressure was found to be higher than free-stream static pressure (approximately 30 percent higher at zero angle of attack) and the heat-transfer rate ranged from 0.01 to 0.12 of the heating rate at the stagnation point at zero angle of attack. Where the flow remained attached to the afterbody the heat-transfer rate was much higher, but it dropped rapidly with distance away from the windward ray.

INTRODUCTION

The heat-transfer distribution on the afterbody of the Apollo reentry vehicle is at present one of the more significant unknown aerodynamic design factors. Because adequate theories for predicting the heat transfer to this region are lacking and there is a likelihood of separation on the afterbody, experimental investigations that show the general nature of the flow about the afterbody as

*Supersedes NASA Technical Memorandum X-699 by Robert A. Jones, 1962.

**Title, Unclassified.

well as the heat-transfer distribution are needed. This report presents measured heat-transfer and pressure distributions for the afterbody, measured pressure distributions along the face in the vertical plane of symmetry, schlieren studies, oil-flow patterns, and wake surveys, all obtained in a conventional Mach number 8 wind tunnel. The pressure data on the face were compared with the empirical relation for the velocity gradient used to determine the theoretical stagnation-point heat-transfer rate at zero angle of attack which, in turn, was used as a reference for the afterbody heat-transfer results. The angle of attack was varied from 0° to 55°. The Reynolds number based on face diameter and free-stream properties varied from 0.10×10^6 to 1.36×10^6.

The applicability of these data, which were obtained in an ideal gas, to high flight speeds where real-gas effects are encountered must be considered. For this body, with the exception of areas affected by separated wake flow, the test Mach number was sufficiently high to minimize the influence of Mach number on the results, and the ideal-gas distributions are approximately equal to the real-gas distributions for equilibrium flow about the body (ref. 1). However, the application of these test results to surfaces heated by separated wake flows may not be justified since the effects of interplay of Reynolds number, enthalpy, and Mach number on such phenomena are not presently understood.

SYMBOLS

c	specific heat of wall
c_p	specific heat of air at constant pressure
h	experimental local heat-transfer coefficient
h_s	calculated heat-transfer coefficient of stagnation point at zero angle of attack
l	surface distance between afterbody tangent points (fig. 1)
M_∞	free-stream Mach number
$N_{Pr,w}$	Prandtl number at wall
p	local measured pressure
$p_{t,2}$	calculated pressure at stagnation point behind normal shock
p_∞	calculated free-stream static pressure
R_∞	Reynolds number based on face diameter and free-stream properties
r_a	afterbody radius (fig. 1)

r_c	corner radius (fig. 1)
r_{eff}	effective sphere radius
r_n	nose radius (fig. 1)
s	surface distance measured from center of face (fig. 1)
T_r	recovery temperature
T_w	temperature at wall
t	time
V	local velocity
V_∞	free-stream velocity
x	distance along afterbody surface, measured from tangent point of forward corner and afterbody (fig. 1)
z	vertical distance from afterbody surface to shock wave (fig. 8)
z'	vertical distance from afterbody surface to probe (fig. 8)
α	angle of attack (fig. 1)
θ	angular location of stagnation point (fig. 5)
μ_s	viscosity at stagnation conditions
μ_w	viscosity at wall
ρ	density of wall
ρ_s	density of air at stagnation conditions
ρ_w	density of air at wall conditions
τ	skin thickness
ϕ	angular displacement from windward ray of afterbody (fig. 1)

TEST FACILITY

The tests were conducted in the Langley Mach 8 variable-density tunnel, which is described in reference 2. This tunnel has an axisymmetric contoured nozzle

terminating in an 18-inch-diameter test section and is adapted for transient testing by a model injection mechanism. The stagnation pressures used were approximately 50, 100, 300, and 1,000 lb/sq in. abs with stagnation temperatures from 750° F to 1,050° F, depending on the pressure. The Mach number in the test area was 7.95 ± 0.05 for stagnation pressures higher than 100 lb/sq in. abs. The tunnel has not been calibrated at lower pressures.

MODELS

One heat-transfer model and one pressure model were used for most of the tests. The oil-flow and wake-survey tests were made with the pressure model, and the temperature-sensitive-paint tests were made with a wooden model. A sketch of the heat-transfer model is presented in figure 1. This model was constructed of type 347 stainless steel. Although the thin-walled shell was nominally 0.025 inch thick, the actual thickness varied as much as ±0.005 inch. Therefore thickness measurements accurate to ±0.0005 inch were made at each thermocouple location. Thermocouples of 0.010-inch-diameter iron-constantan wire were spotwelded to the inner surface of the shell in three rows of seven each at $\phi = 0°$, 45°, and 90°. (See fig. 1.) Each wire of a thermocouple pair was spotwelded to the skin about 0.020 inch from the other wire. The leads were brought out through the center of the sting, which was sharpened on both the leading and the trailing edge so as to minimize the flow disturbances. Three stings, identical except for the angle that they made with the center line of the model, were used in these tests. (See fig. 1.)

The pressure model had a thick wall with tubing soldered into holes and then cut off flush with the outside surface. The tubes on the afterbody had an inside diameter of 0.070 inch (see fig. 1 for the locations); the tubes on the face of the model had an inside diameter of 0.040 inch (locations are shown by symbols in fig. 3).

TEST TECHNIQUE AND DATA REDUCTION

Heat-transfer data were obtained by using a transient testing technique. The tunnel was started and brought to the desired operating conditions, and then the model was rapidly injected into the airstream by a pneumatic piston. The time required for the model to pass through the tunnel boundary layer and for steady flow over the model to be established was about 0.05 second. The thermocouple outputs were recorded 40 times per second by a Beckman 210 high-speed analog to digital data recording system.

Heat-transfer coefficients were obtained by fitting a second-degree curve to the temperature-time data by the method of least squares and computing the time derivative of temperature on a card-programed computer. The heat-transfer coefficient is given by the equation

$$h = \frac{\rho c \tau \frac{dT_w}{dt}}{T_r - T_w} \qquad (1)$$

where the temperature potential $T_r - T_w$ was taken to be the calculated recovery temperature minus the measured wall temperature. The recovery temperature was calculated by assuming a laminar recovery factor of 0.85 and isentropic expansion of the flow from the stagnation point to the local wall pressure. The local wall pressure used was the measured pressure for $\phi \leq 90^\circ$ at the highest value of Reynolds number. No measurements of pressure were made at lower Reynolds numbers or for the case of $\phi > 90^\circ$; for this case ($\phi > 90^\circ$) the pressure was assumed to be the same as the measured value at zero angle of attack, as these pressures were thought to be of the same order and the heat-transfer coefficient was rather insensitive to a small change in recovery temperature.

The heat-transfer coefficients were computed for the time interval from 0.1 to 1.0 second after injection of the model into the airstream. These short times, together with temperature-rise rates of 20° per second or less, resulted in a nearly isothermal surface. Conduction along the skin of the model was therefore estimated to be negligible.

The heat-transfer data are presented as h/h_s, where h is the experimental local value and h_s is the theoretical value for the stagnation point at zero angle of attack. The value of h_s was computed by the method of reference 3:

$$h_s = 0.768 \frac{c_p}{778}\left(N_{Pr,w}\right)^{-0.6}\left(\rho_w \mu_w\right)^{0.1}\left(\rho_s \mu_s\right)^{0.4}\left(\frac{dV}{ds}\right)^{0.5} \qquad (2)$$

where dV/ds, determined by the method of reference 4, was found to be 1.19 times the value of the Newtonian velocity gradient of a sphere of radius r_n.

Pressure data were obtained by photographing a butyl phthalate manometer. These data were obtained at a stagnation pressure of 1,000 lb/sq in. abs. which resulted in a minimum measured pressure of approximately 5 mm Hg abs. Since tunnel operating time is limited to about $1\frac{1}{2}$ minutes, special care was taken to avoid errors which might result from the time required for the manometer to settle out. The settle-out time was minimized by evacuating the tunnel, manometer, and connecting tubing prior to a run to a pressure approximately equal to the one to be measured. Then, as a check, the final pressure was approached with the initial pressure in the system slightly higher than the final pressure for some runs and slightly lower than the final pressure for other runs.

The pressure data are presented as the ratio $p/p_{t,2}$, where p is the local measured value and $p_{t,2}$ is the calculated value at the stagnation point behind a normal shock at a nominal Mach number of 7.95.

RESULTS AND DISCUSSION

Schlieren Photographs

Schlieren photographs of the flow about the model are presented in figure 2 for various combinations of angles of attack and stings. In all of these photographs the thermocouples were located on the top portion of the afterbody. Figure 2(a) shows some of the combinations used to obtain data for $0^\circ \leq \phi \leq 90^\circ$ and figure 2(b) shows some of the combinations used to obtain data for $90^\circ \leq \phi \leq 180^\circ$. The shock standoff distance at zero angle of attack was approximately constant for values of θ less than 20°. The measured standoff distance was compared with the values obtained from the theories of references 5 and 6. Both theories predicted the same detachment distance for spheres of radius r_{eff}. The value of r_{eff} used for this comparison was obtained by the method of reference 4. The value of shock standoff distance predicted by the theories was approximately 10 percent less than the measured value.

Face Pressure Distributions

Pressure distributions along the face in the vertical plane of symmetry are presented in figure 3. Theoretically the ratio $p/p_{t,2}$ should be unity at the stagnation point; however, a nominal Mach number of 7.95 was used to compute $p_{t,2}$ and therefore the discrepancies between theoretical and measured values at the stagnation point are due to differences between the nominal and actual Mach numbers. At an angle of attack of 0° the stagnation-point velocity gradient was determined from the data of figure 3(a) by first adjusting the ratio $p/p_{t,2}$ to go through unity at the stagnation point and then computing the velocity and reading the slope of the velocity curve. This gave a nondimensional stagnation-point velocity gradient of

$$\left(\frac{dV/V_\infty}{ds/r_n}\right)_{s/r_n=0} = 0.31$$

The stagnation-point velocity gradient obtained by Newtonian theory for a sphere with a radius equal to the effective radius found by the method of reference 6 resulted in a value of

$$\left(\frac{dV/V_\infty}{ds/r_n}\right)_{s/r_n=0} = 0.273$$

This value was approximately 13 percent lower than that obtained from the measured pressures. The value obtained by Newtonian theory for the actual spherical radius of the nose was 0.23.

The range of pressures encountered at angles of attack of 27.5° and 35° (figs. 3(b) and 3(c) was greater than could be covered by the butyl phthalate

manometer. Therefore the data for negative values of s/r_n were recorded on a mercury manometer and have a larger scatter than the rest of the data. The data of figure 3(c) indicate the location of the stagnation point at a value of s/r_n between 0.34 and 0.41 for an angle of attack of 35°.

Flow Field

In order to obtain an indication of the flow pattern on the face, small dots of a mixture of oil and lampblack were placed on the model and then the model was suddenly exposed to the airstream. Photographs of some of the patterns that were obtained are presented in figure 4. As it was difficult to make each dot with the same amount of oil, some dots flowed more than others. This did not affect the flow direction; therefore the surface airflow patterns can be determined from the oil traces. The stagnation-point locations are in the top portion of the photographs and the movement of the stagnation point with angle of attack, as determined from the oil patterns and pressure data, is plotted in figure 5.

Since the flow over the afterbody was believed to be separated, several experiments were conducted to determine whether it was separated and, if so, where separation occurred. The technique of placing individual dots of oil on the afterbody proved unsuccessful, apparently because there was insufficient surface shear in the separated region to flow the oil. However, when the entire afterbody was covered with oil the oil appeared to flow forward and to accumulate along a line presumed to be the separation line. A photograph of such a pattern made at zero angle of attack is presented in figure 6. A rather prominent line of accumulated oil can be seen just downstream of the point where the surface was tangent to the free-stream flow direction. In addition to the forward flow of oil believed to be caused by the reverse flow in the separated layer, there was a downward flow around the afterbody believed to be the result of gravity.

Another technique used was to observe the trajectory of small drops of oil ejected from an orifice located about midway on the afterbody of the pressure model. Oil was fed to the orifice through a tube which extended outside the tunnel. The small diameter of the tube and the manner of introducing the oil resulted in a very slow flow consisting of individual drops of oil separated by small air columns. As a drop of oil approached the afterbody orifice, the expanding column of air apparently ejected or blew the drop out into the separated flow region. The motion of the drops as they left the orifice was recorded on 16-mm film at 64 frames per second with strong backlights for illumination. Enlargements made from the 16-mm film, showing the path followed by the oil drops, are presented in figure 7(a). Note that the paths indicate the presence of reverse flow in the separated region.

Also shown in figure 7 are photographs of a tuft study. The tufts were made of cotton string held in holes in the model by wooden wedges. Here again reverse flow was evident, and the tuft located at the rear of the model indicated the presence of a stagnation point at the rear. In order to see how far downstream this reverse flow persisted, a small-diameter wire was stretched across the test section perpendicular to the free-stream flow and a string was attached directly behind the model on its extended center line. Although the string fluttered

violently and was soon destroyed, it showed that reverse flow continued for a distance of at least one-half the face diameter downstream of the rear of the model at zero angle of attack.

A total-head tube was used to make a pressure survey in the wake of the model at zero angle of attack in order to determine the angle between the separated boundary layer and the free-stream flow direction. The results are shown in figure 8(a) for a survey along a vertical line near the rear of the afterbody and in figure 8(b) for a survey along a vertical line near the front of the afterbody. The separation line was assumed to lie somewhere along the dotted portion of the curve, and the angle between the separation line and the free stream was between 9° and 11°. This angle was also determined from the oil pattern of figure 6, from the oil-ejection traces of figure 7(a), and from the measured afterbody pressures. To obtain this angle from the traces of figure 7(a), it was assumed that the separation line could be located by the corner of the model and the highest point reached by the oil drop before it was swept downstream. To obtain this angle from the measured afterbody pressures it was assumed that the sonic point was located on the corner where the tangent to the surface made a 45° angle with the free stream and that the flow went through a two-dimensional Prandtl-Meyer expansion from Mach 1 at this point to the measured afterbody pressure. All these methods gave a value between 9° and 11° for the separation angle.

When the model was at angles of attack other than zero the separation angle became more difficult to determine, particularly on the windward side of the afterbody, as the separation layer on this side became thinner. It was thought, however, that the flow always separated approximately 10° downstream of the point where the surface became tangent to the free stream. One basis for this conclusion was the oil-flow pattern on the afterbody at high angles of attack. Photographs of two such patterns are presented in figure 9. There was a definite lack of oil flow beyond a line approximately 10° downstream of the tangent to the free stream but a considerable oil flow ahead of this line. In addition there was a tendency for the oil to accumulate at this approximate boundary.

Afterbody Pressure Distributions

The measured afterbody pressures are presented in figure 10. Pressure data were obtained only for the windward half of the afterbody ($\phi \leq 90°$) and only for a Reynolds number of 1.36×10^6, which corresponds to the highest stagnation pressure used for these tests. The data for zero angle of attack (fig. 10(a)) show an unexpected variation in pressure with angular location ϕ around the afterbody. This variation was believed to be due to interference caused by the presence of the sting. Data were taken at zero angle of attack with stings 1, 2, and 3 and with a 1/8-inch-thick plate soldered to each side of sting 2 to give a 70-percent increase in sting thickness, but no significant differences in the pressure level or the variation of pressure with ϕ were noticed. It was thought that the sting caused asymmetry in the separated flow and that this asymmetry extended around the entire afterbody, causing the variation of pressure with ϕ at zero angle of attack; however the effect of the sting on the level of the pressure data at low angles of attack was not known. At angles of attack of 0° and 5° the measured afterbody pressures were about 30 percent higher than the free-stream static pressure.

Reference 7 presents measured afterbody pressure distributions for this same shape at a Mach number of 6 for values of ϕ from 0° to 180°. The pressure levels reported therein for the separated region were less than free-stream static pressure, and at zero angle of attack the afterbody data of reference 7 are approximately 50 percent lower than the data of the present investigation. The sting used in the tests of reference 7 was entirely different, being round in cross section with its center line parallel to the model center line but displaced from it a distance of about 1/5 the face diameter. A change in Mach number from 6 to 8 is believed to have only a small effect on afterbody pressure coefficients for the same configuration. Therefore the difference in afterbody pressure level between reference 7 and this investigation indicates that the method of supporting the model had a significant effect on data obtained in the separated region of the afterbody.

Another result reported in reference 7 was that the pressure in the separated region decreased with an increase in angle of attack. A similar variation was found in the data of figure 10 for $\phi = 90^\circ$ at angles of attack greater than 5°. At angles of attack between 35° and 55° the pressure at $\phi = 90^\circ$ was approximately equal to the free-stream static pressure.

In general, the pressure in the separated region (fig. 10) was constant (independent of the x/l location); however at an angle of attack of 15° the distribution along the windward ray varied from a low at $x/l = 0.13$ to a maximum at $x/l = 0.85$. The cause of this variation is not understood. At an angle of attack of 25° the angle between the free stream and the windward ray of the afterbody was 10°. This was the borderline case for separation and it was not determined whether the flow along the windward ray was attached or separated, but there was a significant increase in pressure level along this ray. At an angle of attack of 35° the windward ray of the afterbody was alined parallel to the free stream. The pressure near the forward corner was much higher than the Newtonian value, and although the pressure rapidly decreased toward the rear of the model at $x/l = 0.85$, it was still much higher than the Newtonian value. At higher angles of attack there was still a rapid decrease in pressure along the windward ray toward the rear. At $\alpha = 45^\circ$ the pressure almost reached the Newtonian value at the rear orifice, and at $\alpha = 55^\circ$ the pressure fell 12 percent below the Newtonian value at this location.

Afterbody Heat-Transfer Distributions

The variation of the heat-transfer-coefficient ratio h/h_s with distance along the windward ray of the afterbody is shown in figure 11 for four values of Reynolds number. The theoretical value at the stagnation point at zero angle of attack, h_s, was computed by using the method of reference 2 and the stagnation-point velocity gradient of reference 4. The stagnation-point velocity gradient predicted by reference 6 was about 13 percent below that determined from the measured pressure data of figure 5. A 13-percent error in velocity gradient would make a difference in h_s of less than 4 percent.

Note the change in heat-transfer distribution with angle of attack in figure 11. At $\alpha = 0^\circ$ and 5°, the heating increased somewhat with distance; at 15° and 25° it was almost constant; at 35° it initially decreased with distance and

then leveled off at an x/l value of about 0.6; and at the highest angle of attack it decreased to an x/l value of 0.4 and then increased again. At zero angle of attack there was a much more rapid increase in heat transfer with distance from the corner at the highest Reynolds number (1.36×10^6) than at the lower Reynolds numbers. This increase was thought to be the result of interference from the sting. Thermocouples were placed on three different rays of the afterbody ($\phi = 0^\circ$, 45°, and 90°) and a variation in heat-transfer distribution with ϕ was found at zero angle of attack. This variation was due to the same sting interference that affected the pressure data at $\alpha = 0^\circ$; however the effect of this interference on heat transfer was larger. The results of tests made to study the magnitude of this interference and the region influenced by it are shown in figures 12 and 13.

Figure 12 shows the variation of heat transfer with ϕ at $\alpha = 0^\circ$ for different stings at three Reynolds numbers. In figure 12(a) the data for $\phi = 0^\circ$ are the same as the data of figure 11(a) for $\alpha = 0^\circ$; but also included are data for $\phi = 45^\circ$ and $\phi = 90^\circ$. The variation of h/h_s with ϕ was apparently caused by the asymmetry of the separated flow due to the sting, and a large increase in heating rate was indicated at the highest Reynolds number. The variation of heating rate with ϕ for large values of x/l was much greater than for small values of x/l, indicating less sting effect on the forward portion of the afterbody. A similar plot of data taken with sting 3 at $\alpha = 0^\circ$ is shown in figure 12(b). Here again interference effects are evident, though they are not as great as with sting 2. Tests were also made with sting 3 and roughness on the face of the model, as well as with a thickened sting and no roughness. These results are shown in figures 12(c) and 12(d), respectively. The roughness used consisted of small three-dimensional particles (0.0075 inch) glued in a random distribution over the face. The effectiveness of this roughness in promoting boundary-layer transition was not determined; however the data of figure 12(c) show significantly less variation with both x/l and Reynolds number than the data of figure 12(b). Increasing the thickness of the sting (fig. 12(d)) had an effect similar to that of placing roughness on the face of the model.

A qualitative indication of the effect of this sting interference on the afterbody heating rates was obtained by coating wooden models with a temperature-sensitive paint and photographing the color patterns formed when the model was suddenly injected into and heated by the hot airstream. (See ref. 8.) A sketch of the patterns obtained is shown in figure 13. The paint changed color three times (pink to blue to yellow and finally to olive green). The relative heating rates are indicated by the color of the different areas. The patterns of figure 13 were obtained at the highest Reynolds number (1.36×10^6).

The results of the various tests of sting interference at zero angle of attack indicate that this interference increased the heating rate and, therefore, that the data are conservative. At higher angles of attack more characteristic of the Apollo capsule, sting interference was not encountered on the windward side of the afterbody and was believed to have been much less significant on the leeward side than at low angles of attack.

Another interesting result of the temperature-sensitive-paint patterns of figure 13 was the very narrow yellow band on the corner at or near the separation

line. This indicates that the heating rate right at the point of separation was higher than the rates just upstream and just downstream of that point.

Figures 14 to 17 show the heat-transfer distribution around the afterbody at higher angles of attack. In order to obtain data for values of ϕ greater than 90° the model was tested with the instrumented portion on the lee side of the afterbody. This put the sting on the windward side of the afterbody, as shown in the schlieren photographs of figure 2(b), and resulted in two sets of data for $\phi = 90^\circ$. The data taken with the sting on the windward side are shown by solid symbols in figures 14 to 16. At low angles of attack, where the flow was separated completely around the afterbody, the differences between these two sets of data at $\phi = 90^\circ$ are apparently due to differences in the interference from what was essentially two different stings, both located in the separated region. At angles of attack of 35° or greater, the flow was attached to the windward portion of the afterbody and the data shown by the plain symbols should be free of any interference effects. However, the data shown by solid symbols ($\phi > 90^\circ$) were affected by sting interference, but this interference problem was different from that at low angles of attack since the sting was located in the attached-flow region rather than in the separated region.

The ratio h/h_s for the separated afterbody region at angles of attack was well within the range (0.01 to 0.12) of h/h_s for the separated region at zero angle of attack. On the windward portion of the afterbody at high angles of attack (attached flow) the heating rates were of course much higher, but they dropped rapidly with distance away from the windward ray.

On the basis of the small variation of heat-transfer-coefficient ratio with Reynolds number and on the results of previous investigations made in this tunnel, the flow was thought to be laminar over the entire body except possibly for the tests with roughness on the face of the model and for regions near the juncture of the sting and afterbody.

CONCLUSIONS

Pressure distributions along the vertical plane of symmetry on the face of an Apollo reentry configuration and pressure and heat-transfer distributions on the afterbody were obtained at a Mach number of 8 for angles of attack from 0° to 55° and Reynolds numbers from 0.10×10^6 to 1.36×10^6 based on face diameter. The results indicate the following:

1. The shock standoff distance at zero angle of attack could be predicted within approximately 10 percent by using the theory for spheres and an effective sphere radius for the model.

2. The measured stagnation-point velocity gradient at zero angle of attack agreed within 13 percent with that computed by an empirical method.

3. The flow over the body appeared to separate just downstream of the point where the tangent to the surface became parallel to the free-stream flow. The angle between the free stream and the model surface at the separation line was approximately 10° and was independent of angle of attack.

4. The method of supporting the model could have a significant effect on data obtained in the separated region of the afterbody. The sting variations made in this investigation had considerable effect on the afterbody heating rate at zero angle of attack but did not appear to affect the level of the pressure distributions.

5. The pressure on the separated portion of the afterbody was generally higher than free-stream static pressure (approximately 30 percent higher at zero angle of attack).

6. The heat-transfer rate to the separated portion of the afterbody was within 1 to 12 percent of the value for the zero-angle-of-attack stagnation point for all angles of attack of the investigation. On the windward portion of the afterbody at high angles of attack (attached flow) the heating rates were of course much higher, but they dropped rapidly with distance away from the windward ray.

Langley Research Center,
National Aeronautics and Space Administration,
Langley Station, Hampton, Va., February 28, 1963.

REFERENCES

1. Hayes, Wallace D., and Probstein, Ronald F.: Hypersonic Flow Theory. Academic Press, Inc. (New York), 1959, chs. I and VIII.

2. Jones, Robert A.: Heat-Transfer and Pressure Distributions on a Flat-Face Rounded-Corner Body of Revolution With and Without a Flap at a Mach Number of 8. NASA TM X-703, 1962.

3. Fay, J. A., and Riddell, F. R.: Theory of Stagnation Point Heat Transfer in Dissociated Air. Jour. Aero. Sci., vol. 25, no. 2, Feb. 1958, pp. 73-85, 121.

4. Boison, J. Christopher, and Curtiss, Howard A.: An Experimental Investigation of Blunt Body Stagnation Point Velocity Gradient. ARS Jour., vol. 29, no. 2, Feb. 1959, pp. 130-135.

5. Ridyard, Herbert W., and Storer, Elsie M.: Stagnation-Point Shock Detachment of Blunt Bodies in Supersonic Flow. Jour. Aerospace Sci. (Readers' Forum), vol. 29, no. 6, June 1962, pp. 751-752.

6. Van Dyke, Milton D., and Gordon, Helen D.: Supersonic Flow Past a Family of Blunt Axisymmetric Bodies. NASA TR R-1, 1959.

7. Romeo, David J.: Experimental Results of the Pressure Distribution on a Blunt-Nose Conical-Afterbody Lunar-Mission Spacecraft With Four Nose-Edge Radii for a Mach Number of 6.0 and an Angle-of-Attack Range of 0° to 50°. NASA TM X-705, 1962.

8. Stainback, P. Calvin: A Visual Technique for Determining Qualitative Aerodynamic Heating Rates on Complex Configurations. NASA TN D-385, 1960.

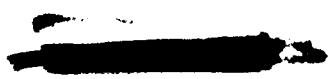

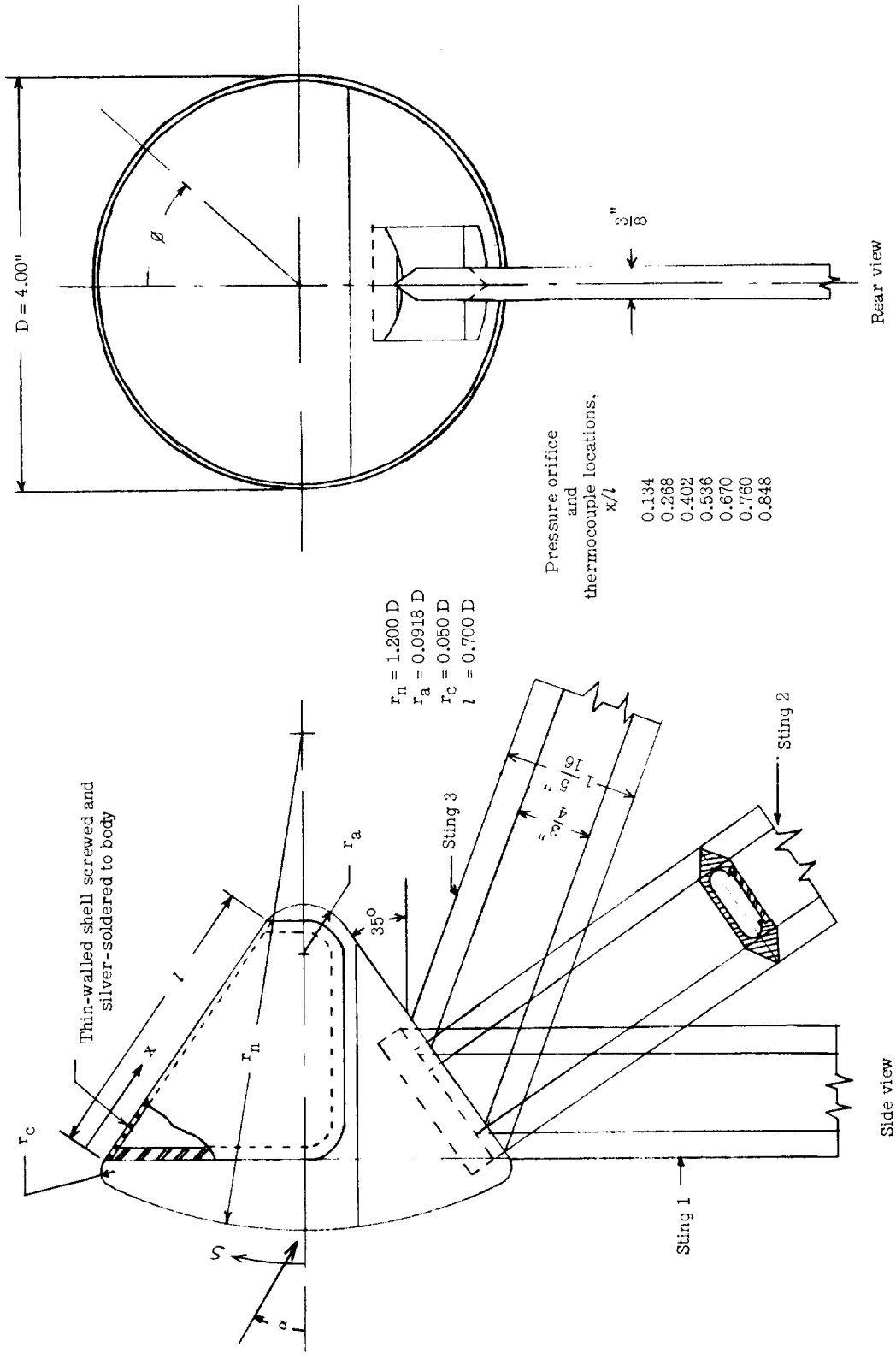

Figure 1.- Sketch of heat-transfer model.

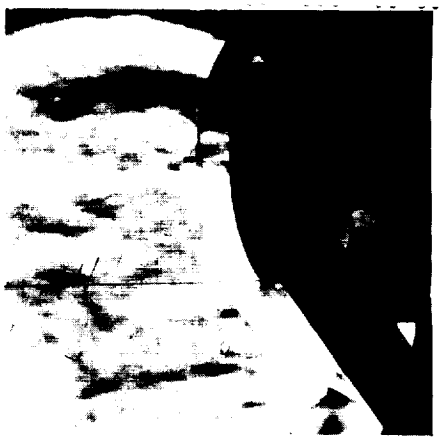

$\alpha = 0^{\circ}$; sting 2

$\alpha = 15^{\circ}$; sting 2

$\alpha = 25^{\circ}$; sting 2

$\alpha = 35^{\circ}$; sting 2

$\alpha = 45^{\circ}$; sting 1

$\alpha = 55^{\circ}$; sting 1

(a) Arrangements used to obtain data for $0^{\circ} \leq \phi \leq 90^{\circ}$. L-62-2058

Figure 2.- Schlieren photographs.

$\alpha = 5^{\circ}$; sting 3

$\alpha = 15^{\circ}$; sting 3

$\alpha = 25^{\circ}$; sting 3

$\alpha = 35^{\circ}$; sting 3

$\alpha = 35^{\circ}$; sting 1

$\alpha = 45^{\circ}$; sting 3

(b) Arrangements used to obtain data for $90^{\circ} \leq \phi \leq 180^{\circ}$. L-63-60

Figure 2.- Concluded.

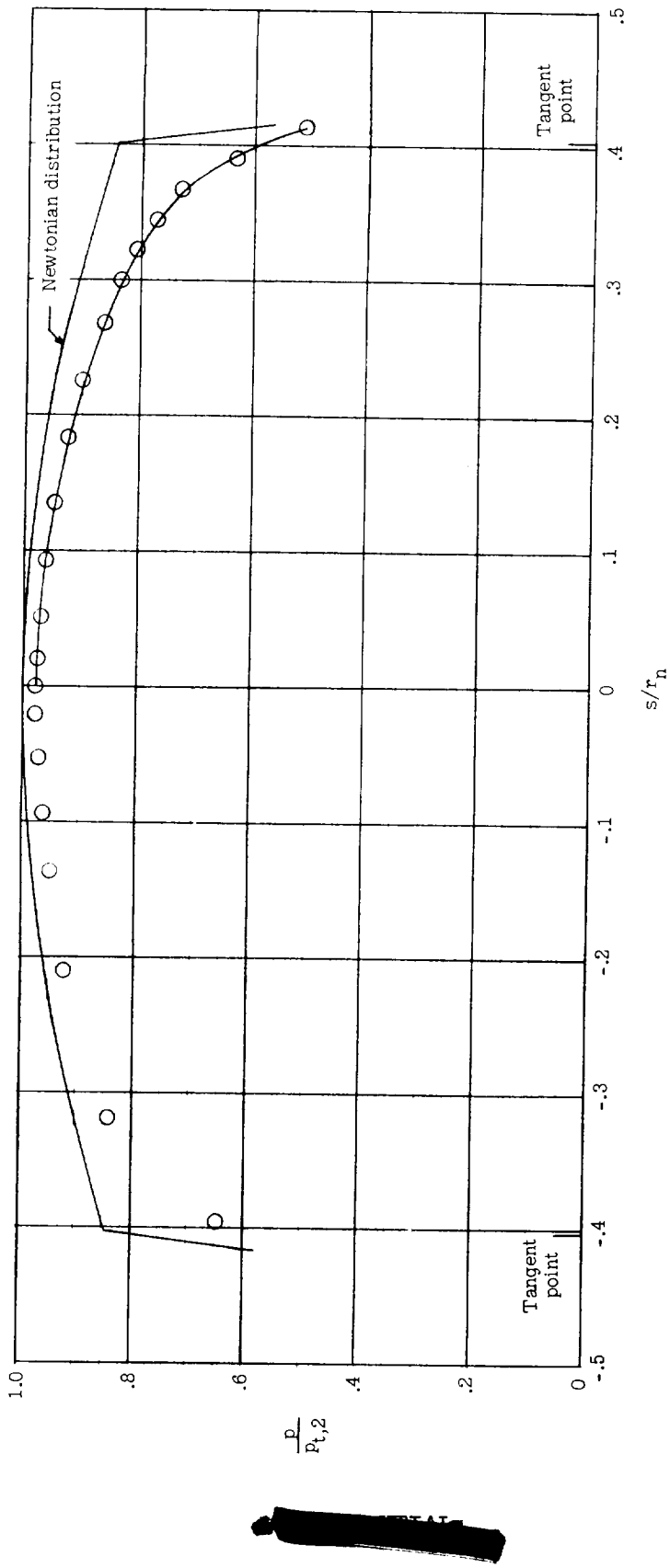

(a) $\alpha = 0^\circ$.

Figure 3.- Pressure distribution on face (vertical plane of symmetry).

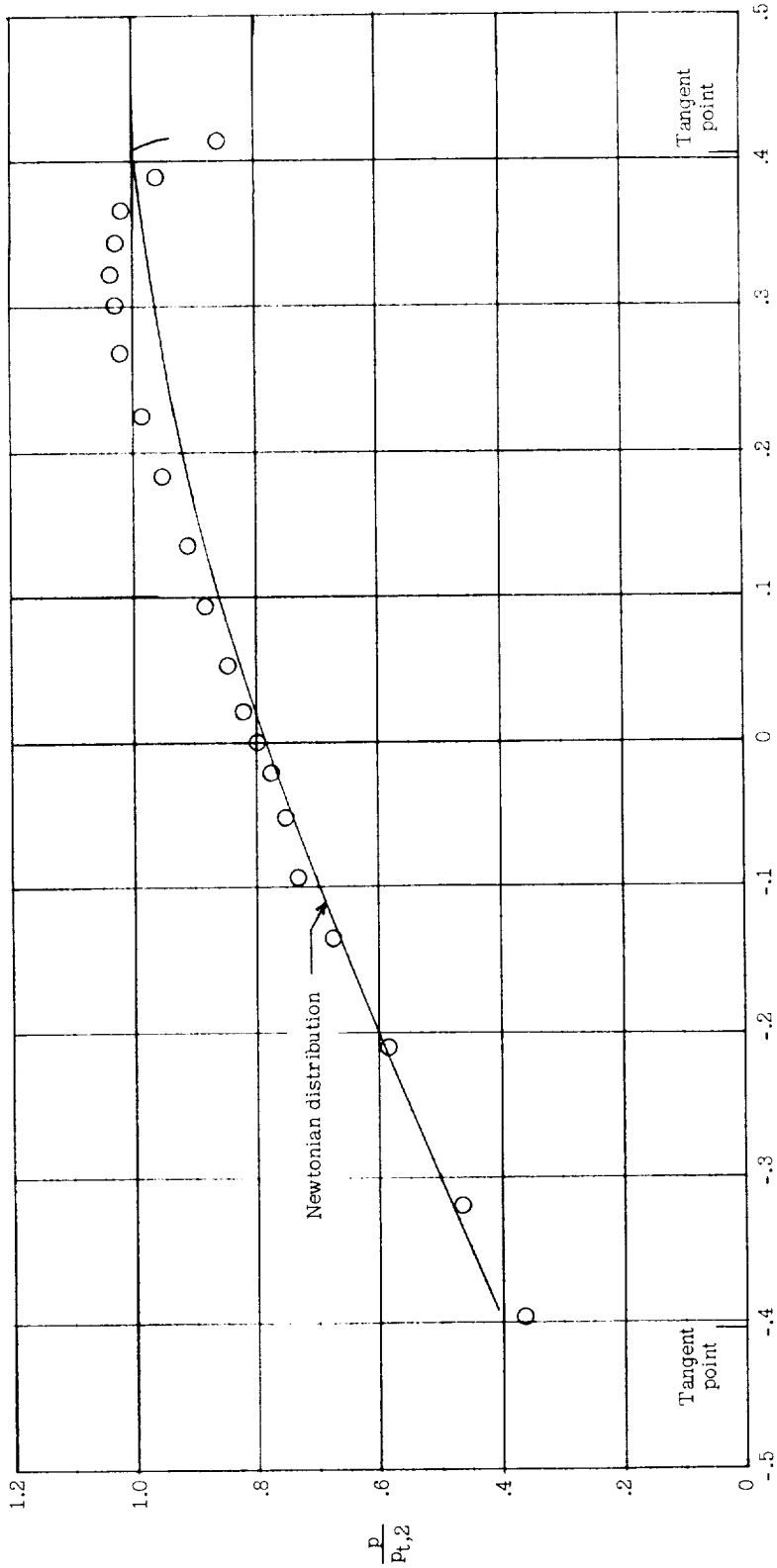

(b) $\alpha = 27.5^\circ$.

Figure 3.- Continued.

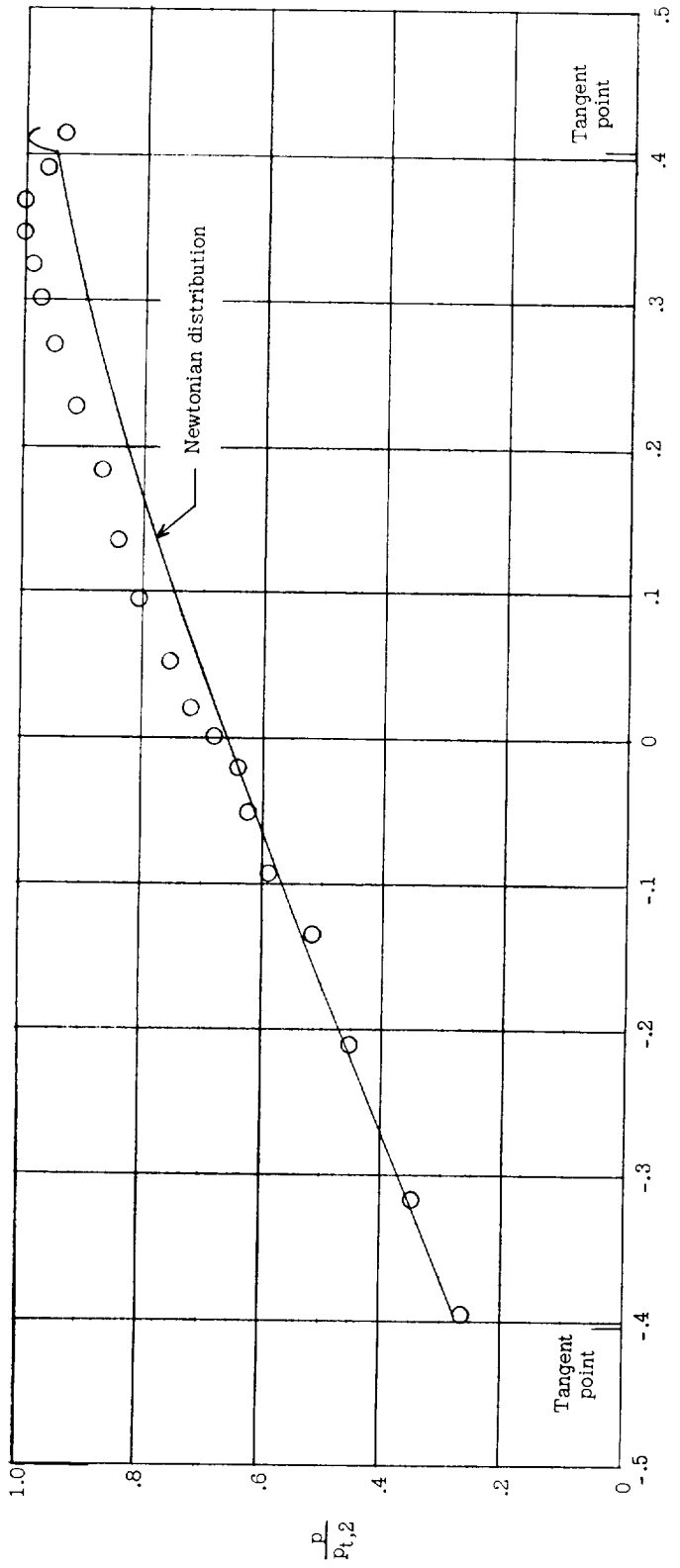

(c) $\alpha = 35^\circ$.

Figure 3.- Concluded.

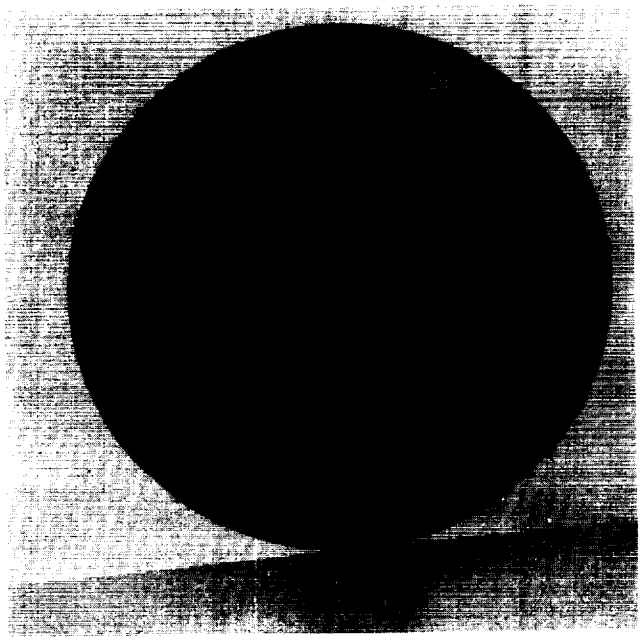

$\alpha = 15^{\circ}$

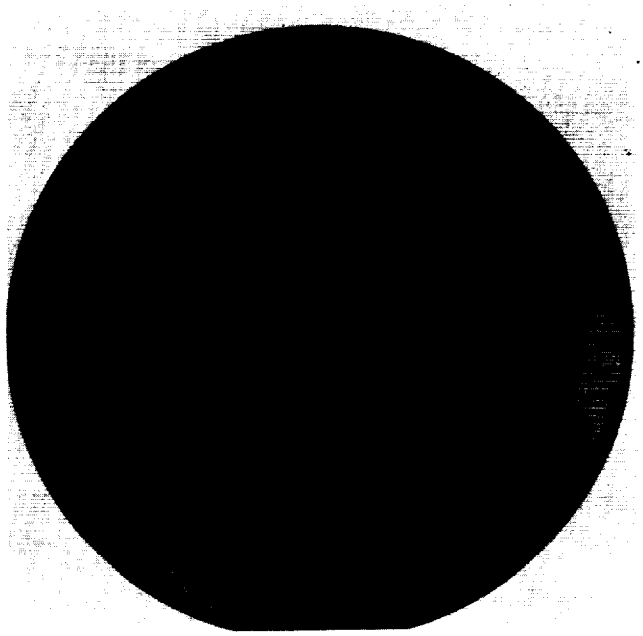

$\alpha = 25^{\circ}$

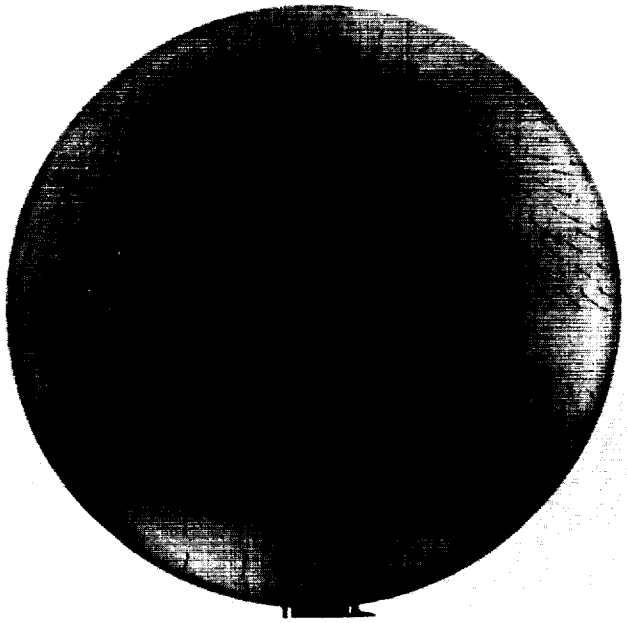

$\alpha = 30^{\circ}$

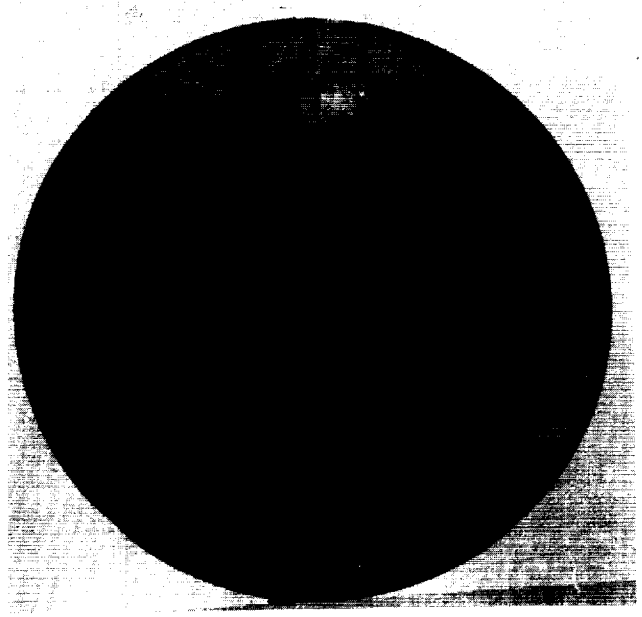

$\alpha = 40^{\circ}$

Figure 4.- Oil-flow patterns on face.

L-63-61

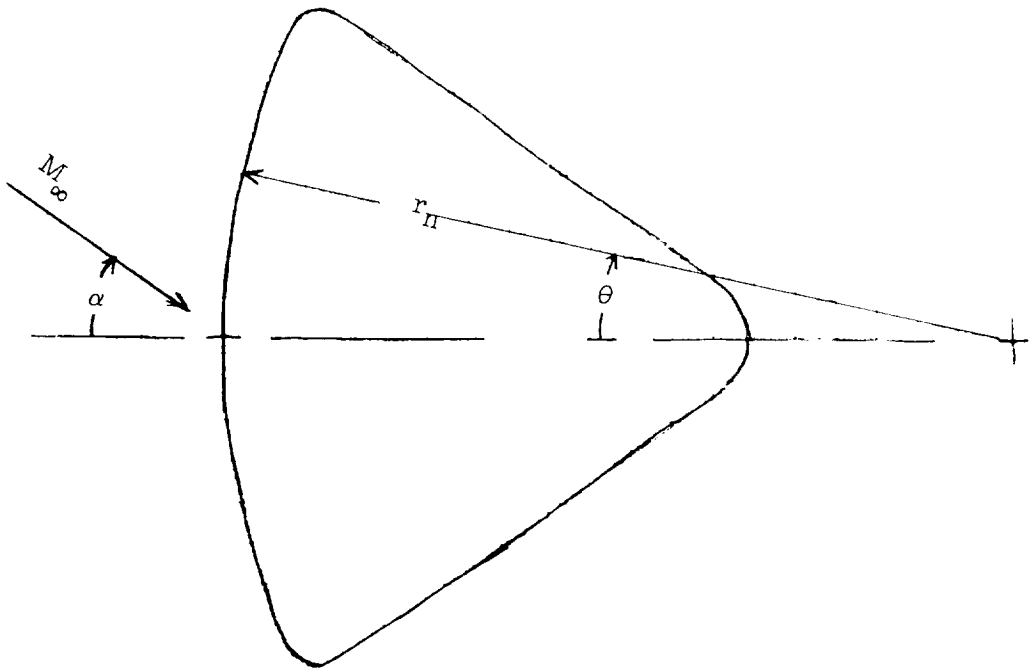

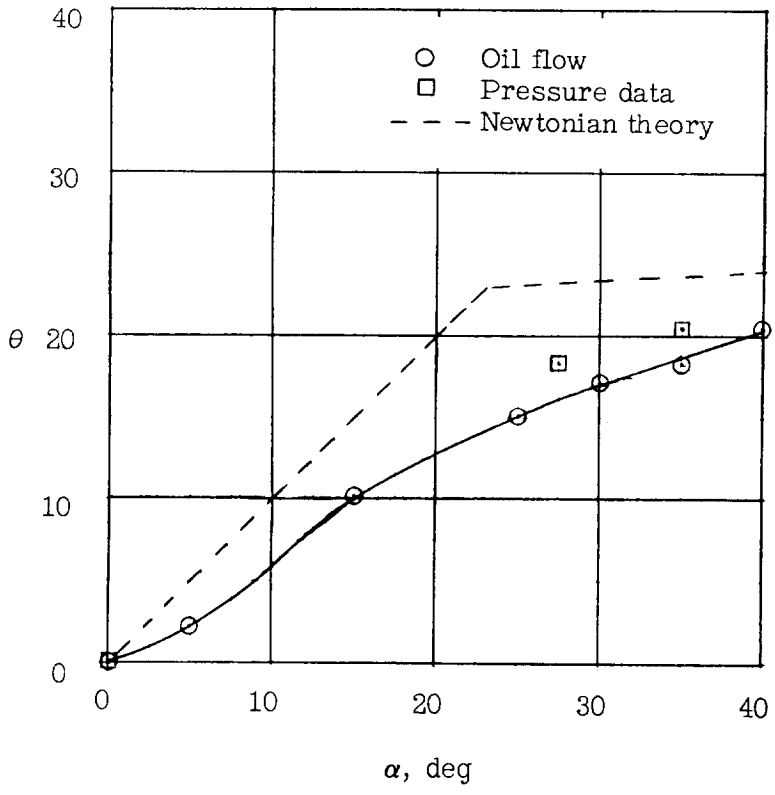

Figure 5.- Movement of stagnation point with angle of attack.

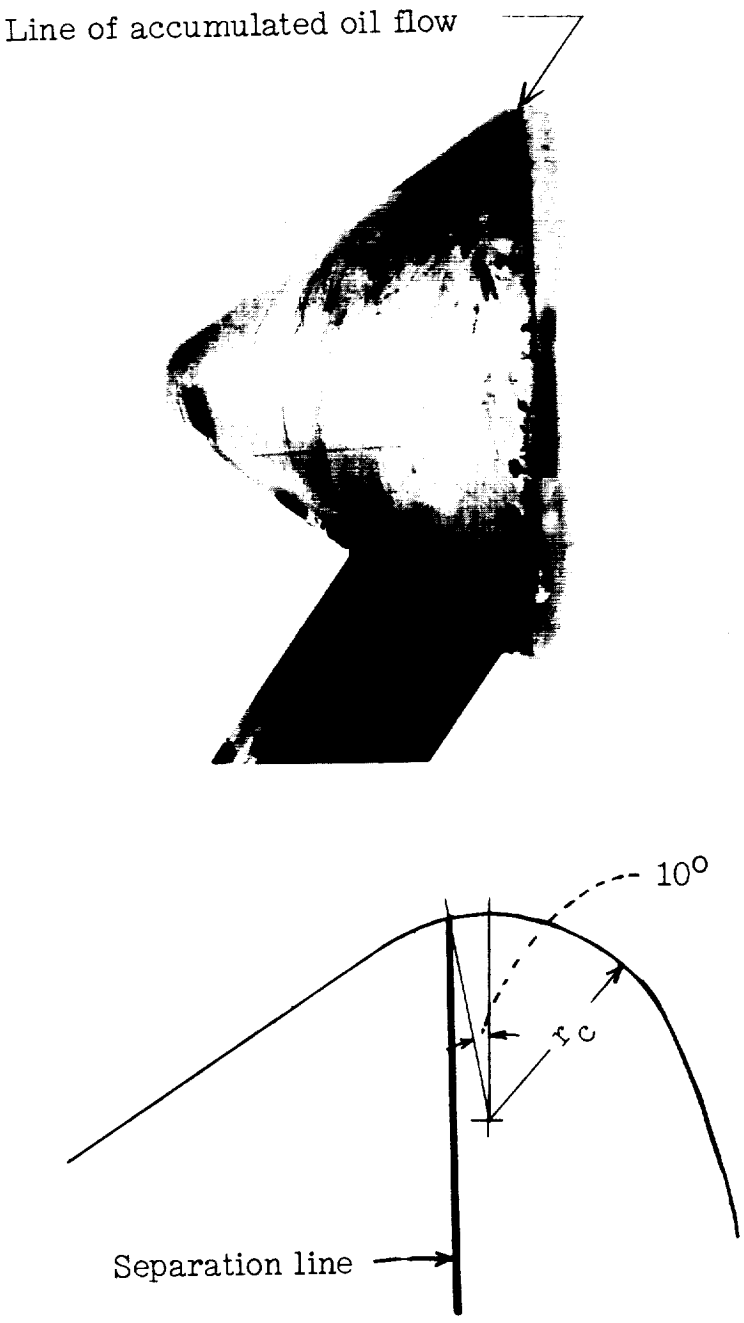

L-63-62

Figure 6.- Photograph and sketch of oil-flow pattern showing separation line at $\alpha = 0^{\circ}$.

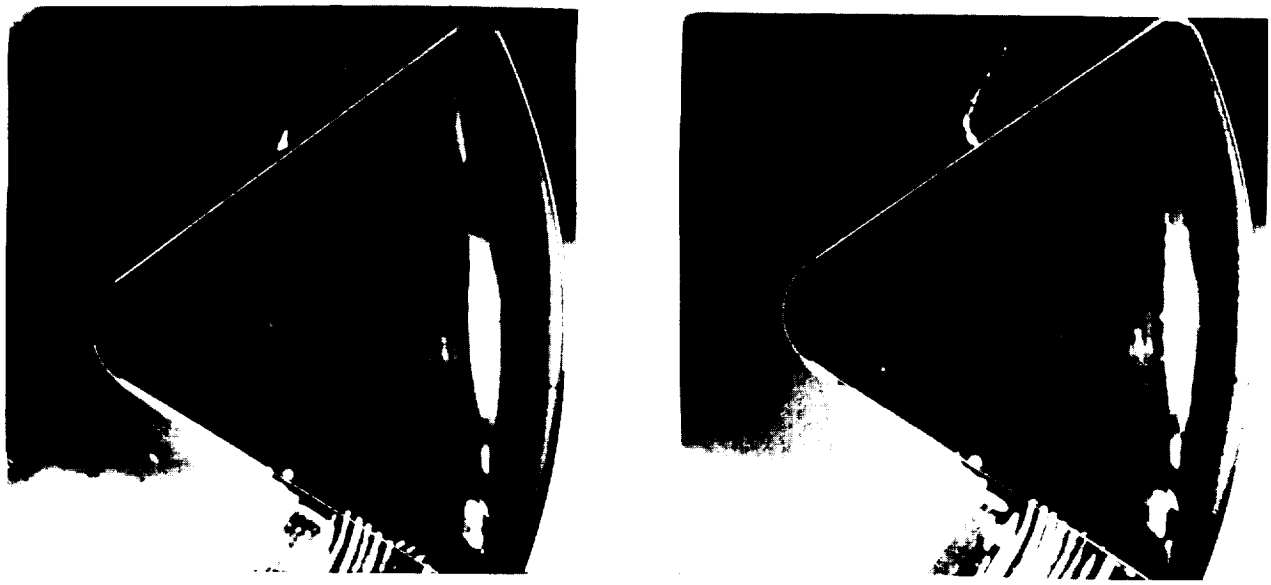

Flow

(a) Oil ejection.

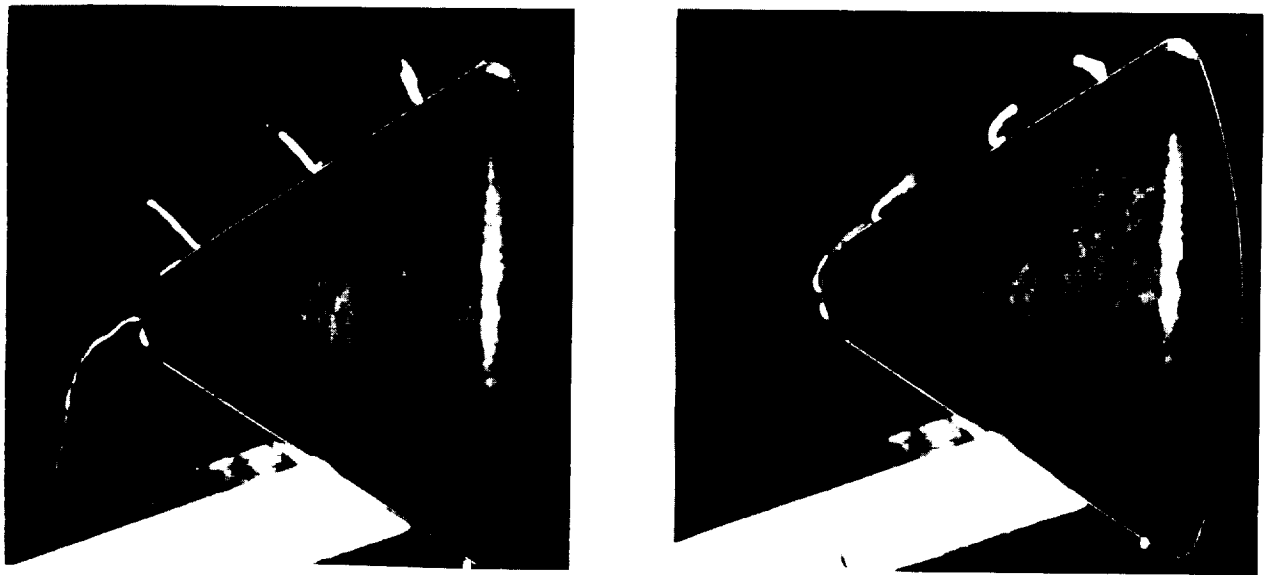

No flow

Flow

Flow

(b) Tuft study.

L-63-63

Figure 7.- Separation studies made at zero angle of attack.

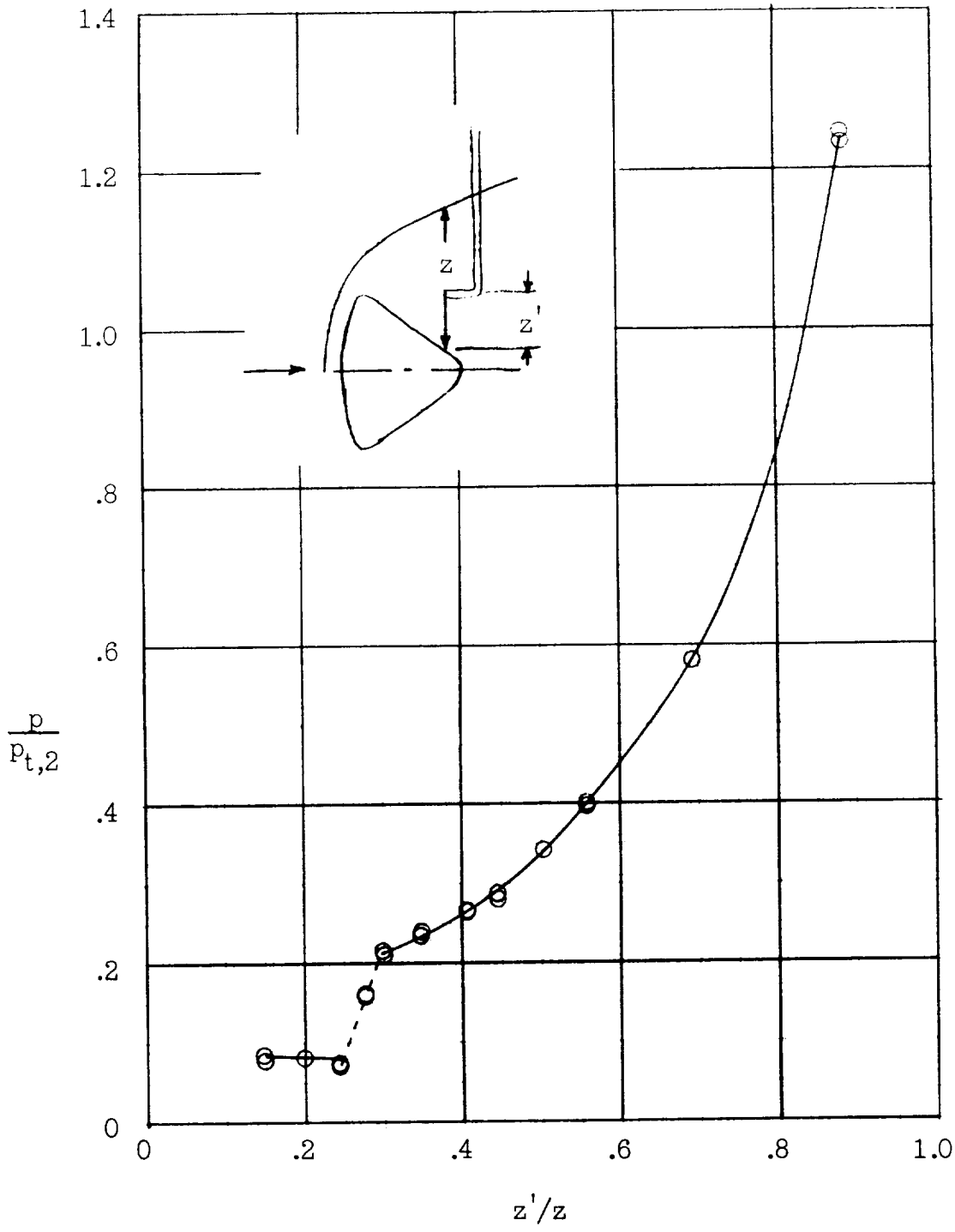

(a) Rearward location.

Figure 8.- Pressure survey in wake. $\alpha = 0^{o}$.

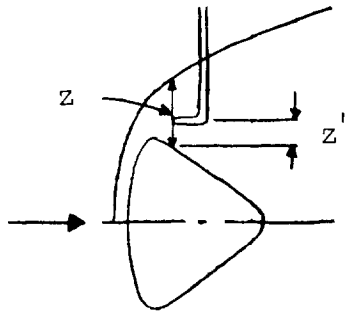

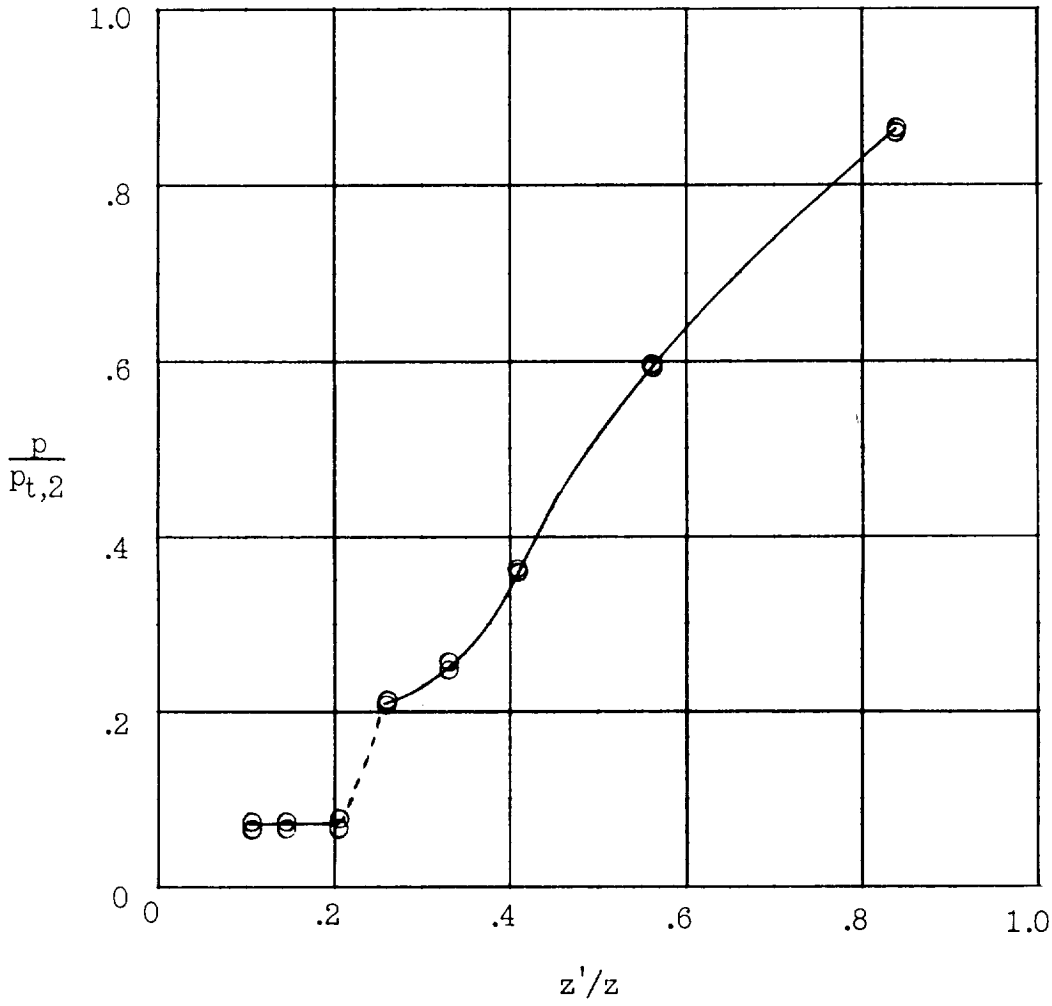

(b) Forward location.

Figure 8.- Concluded.

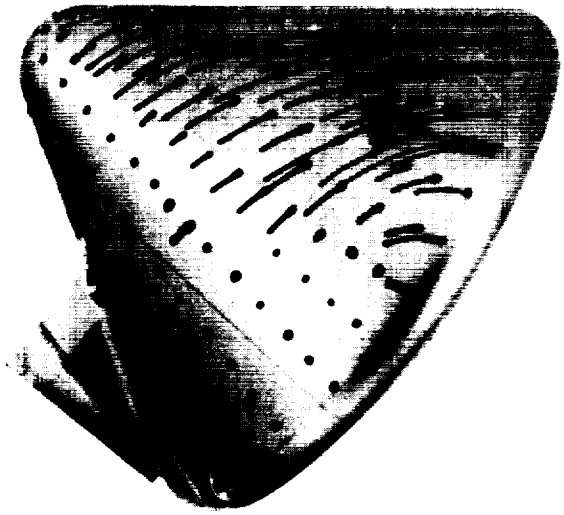

$\alpha = 35^{\circ}$

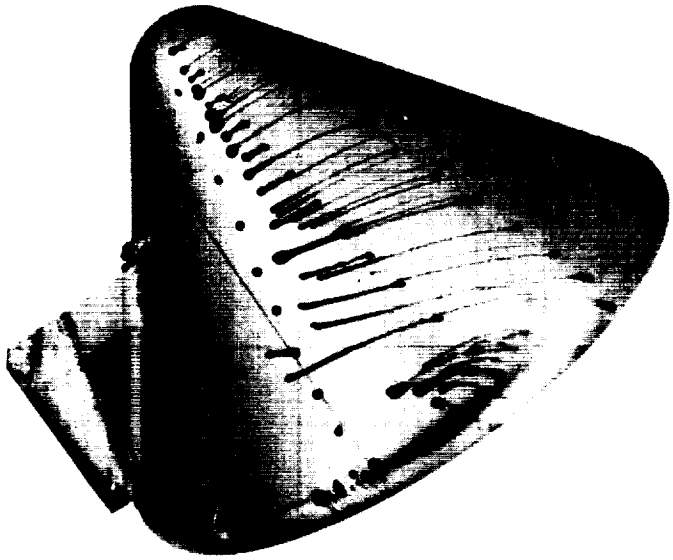

$\alpha = 55^{\circ}$

Figure 9.- Oil-flow patterns on the afterbody at high angles of attack. L-63-64

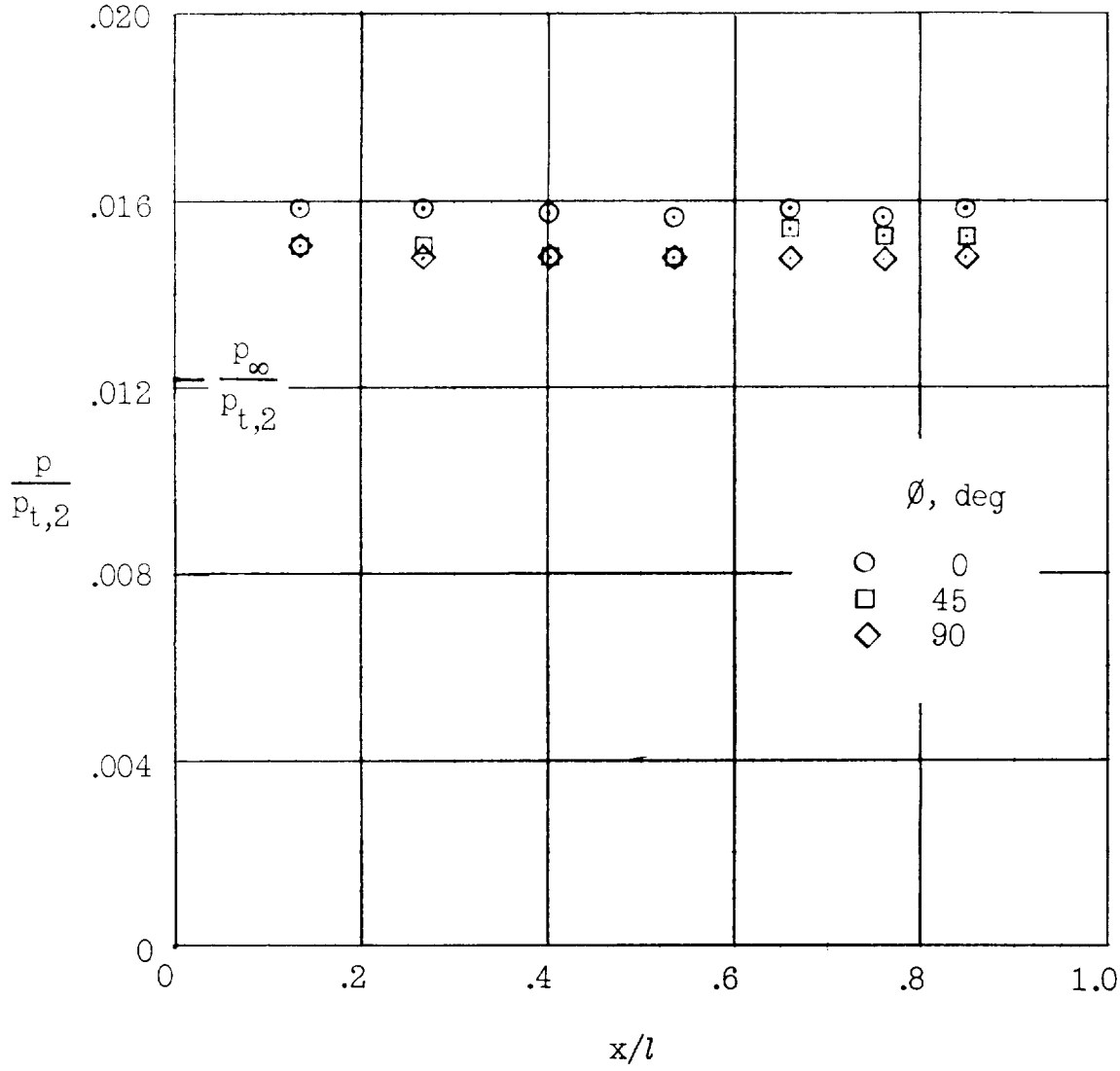

(a) $\alpha = 0^o$; sting 2.

Figure 10.- Afterbody pressure distribution. $R_\infty = 1.36 \times 10^6$.

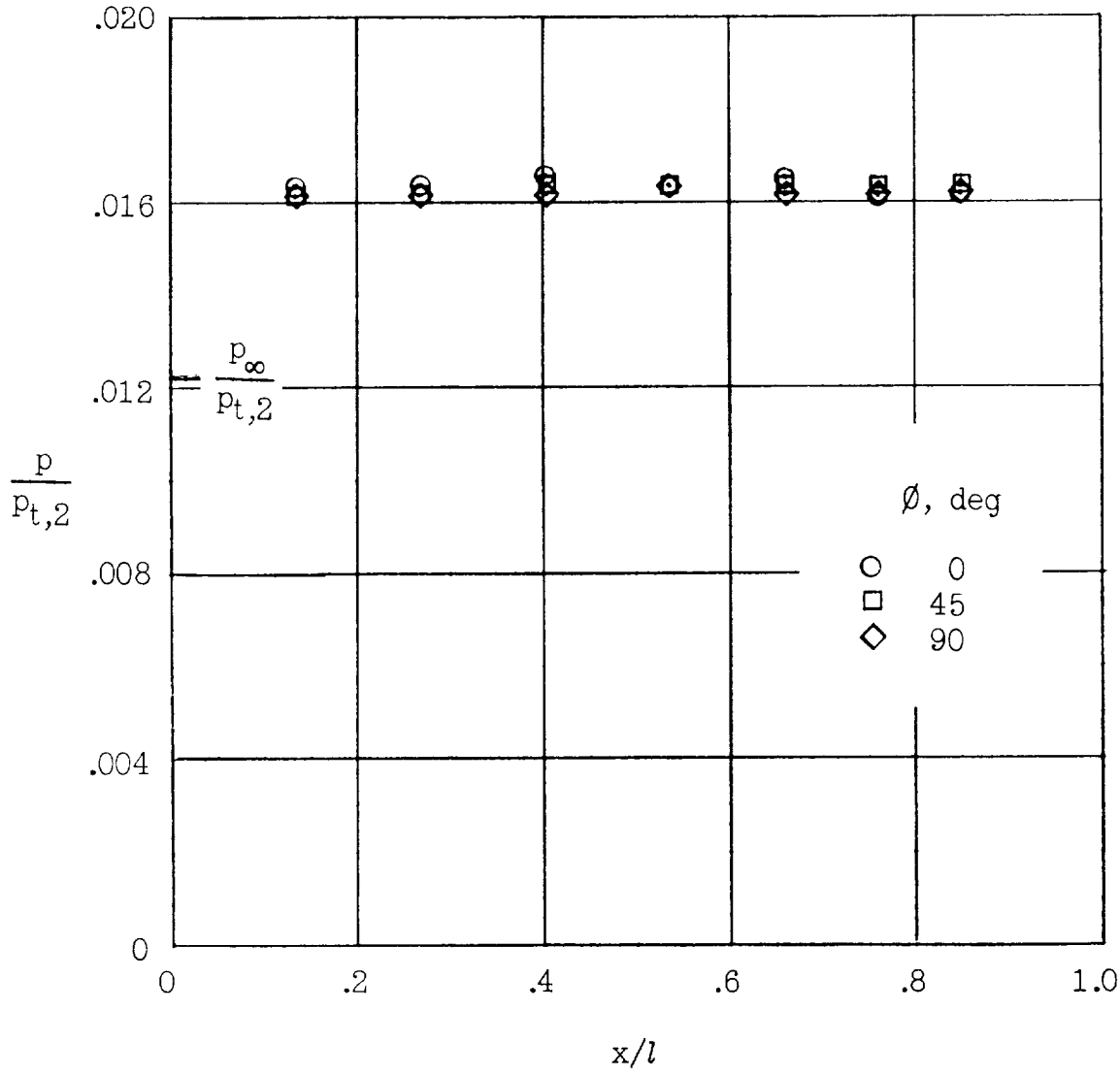

(b) $\alpha = 5^\circ$; sting 2.

Figure 10.- Continued.

[redacted]

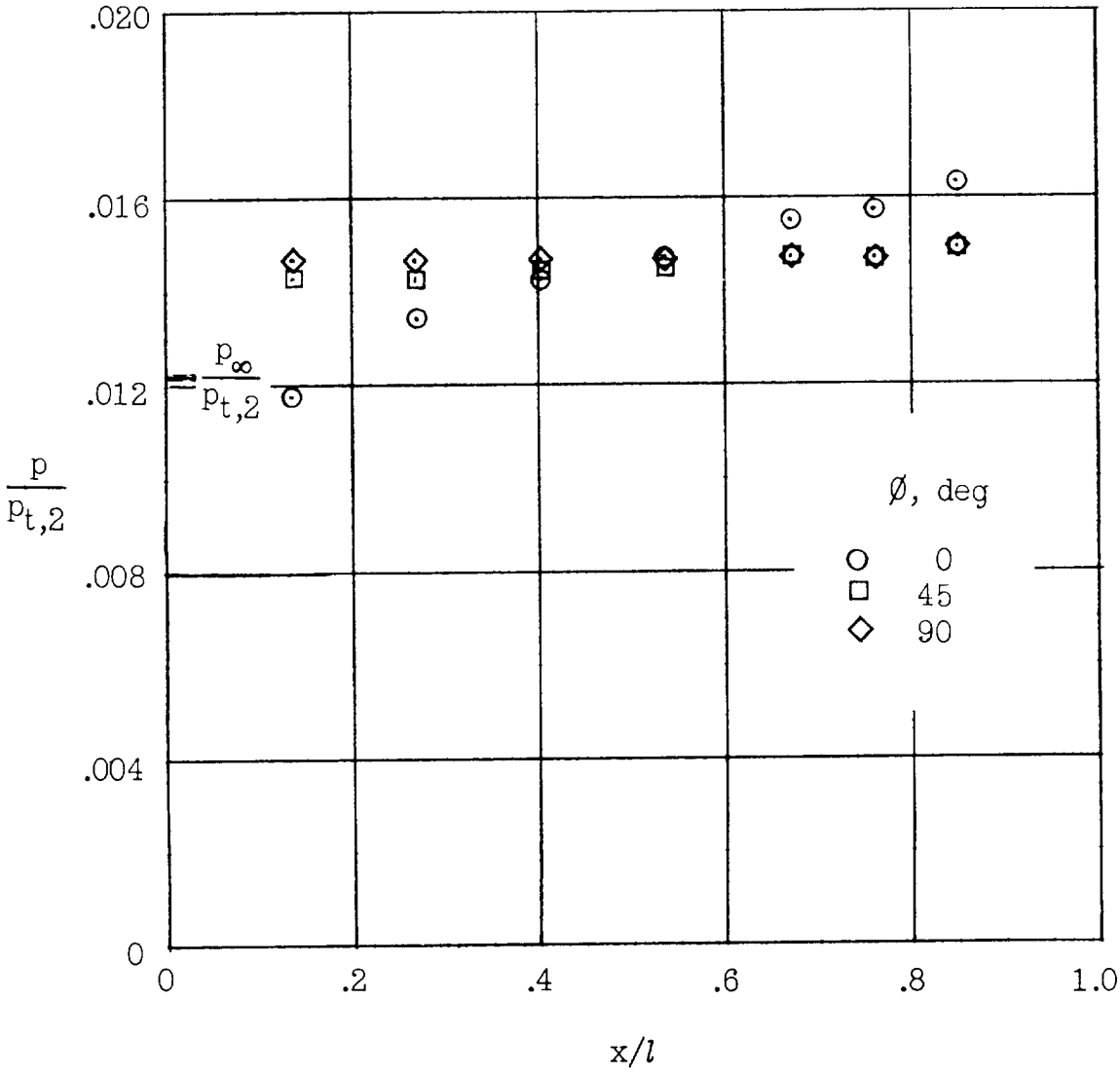

(c) $\alpha = 15^\circ$; sting 2.

Figure 10.- Continued.

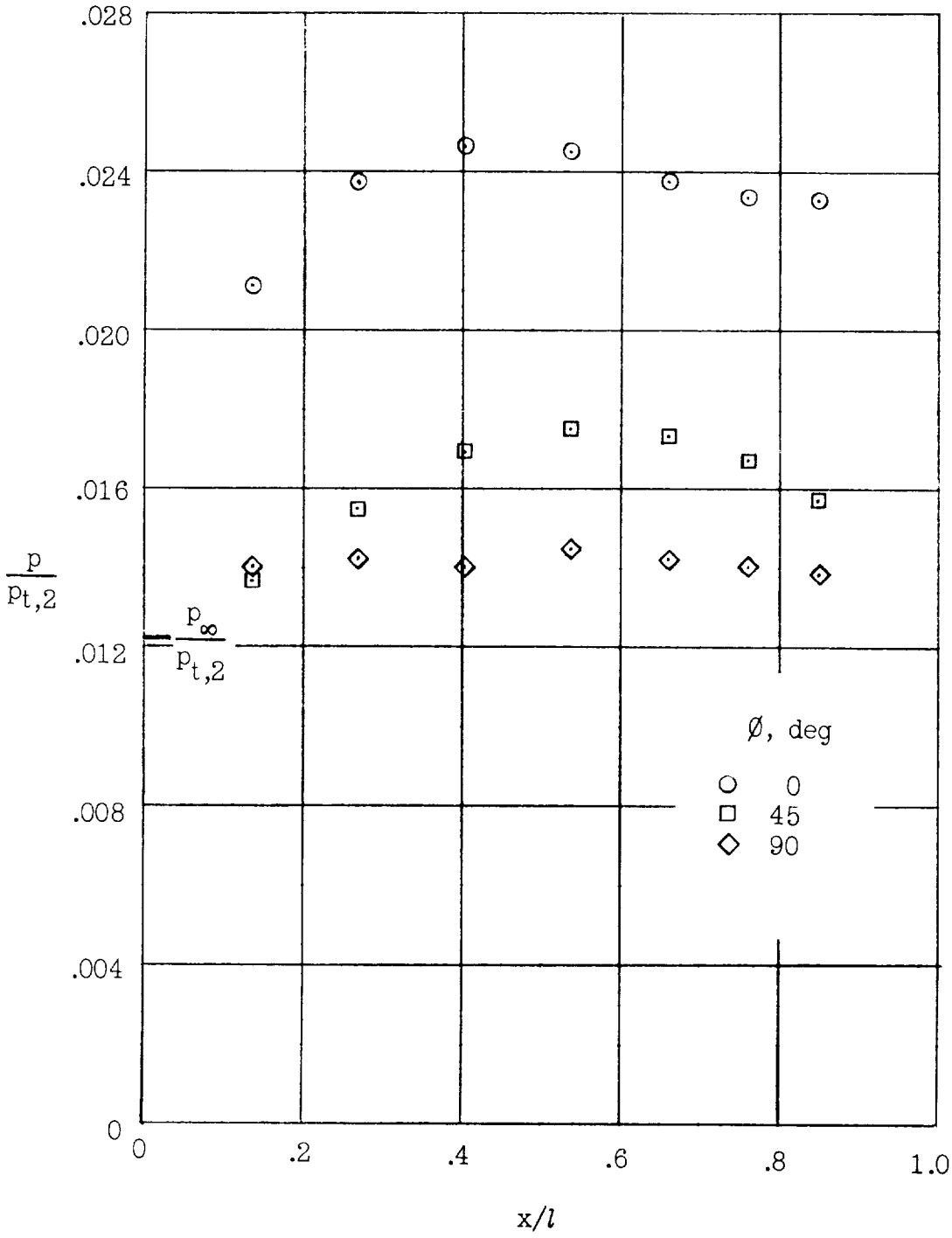

(d) $\alpha = 25^{\circ}$; sting 2.

Figure 10.- Continued.

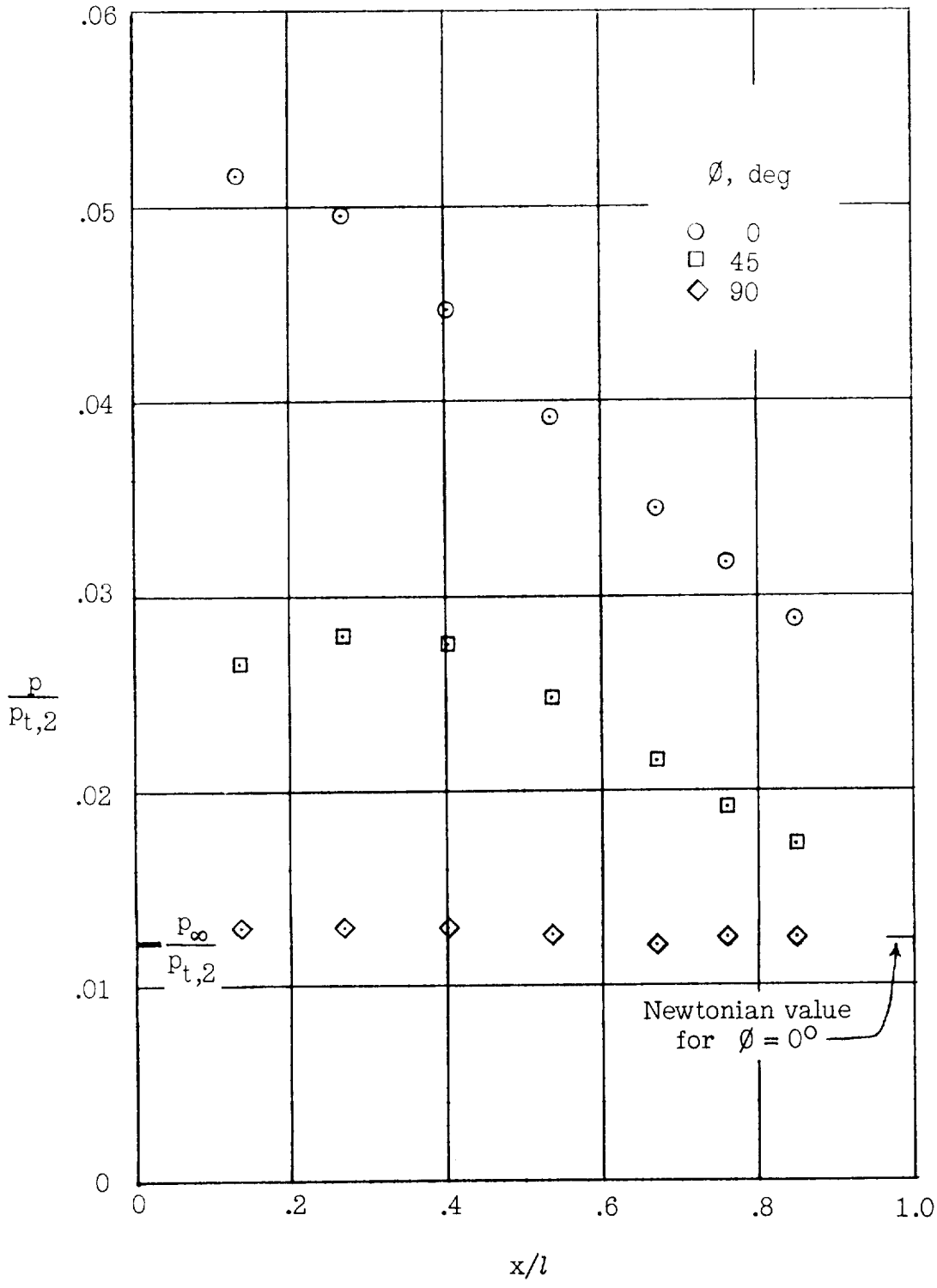

(e) $\alpha = 35^\circ$; sting 2.

Figure 10.- Continued.

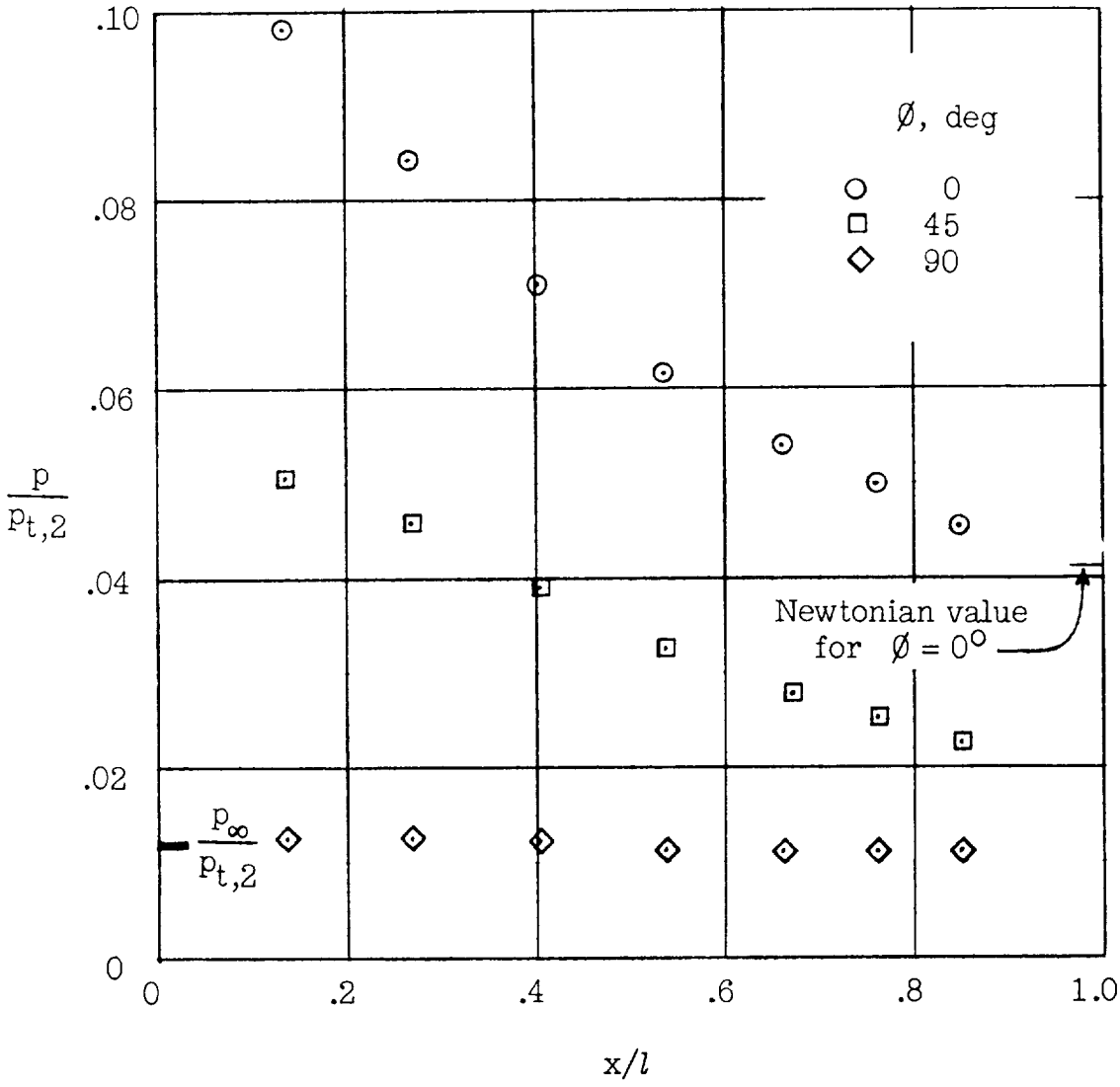

(f) $\alpha = 45^{\circ}$; sting 1.

Figure 10.- Continued.

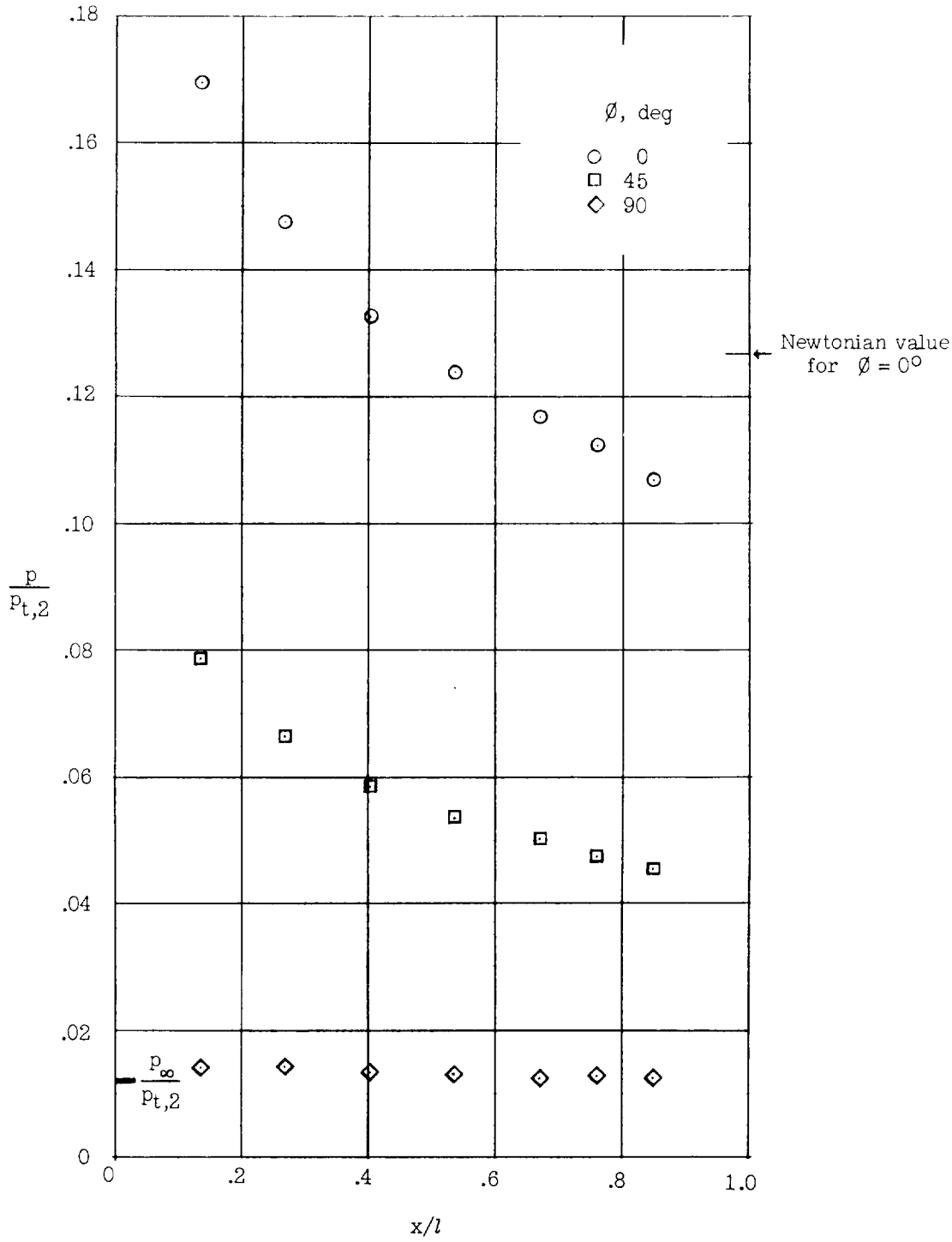

(g) $\alpha = 55^\circ$; sting 1.

Figure 10.- Concluded.

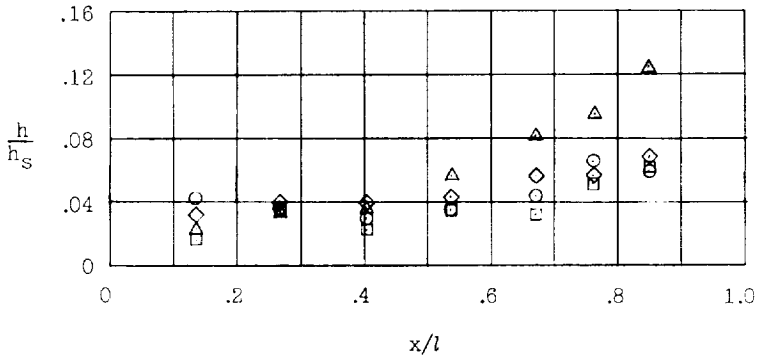

(a) $\alpha = 0^{\circ}$; sting 2.

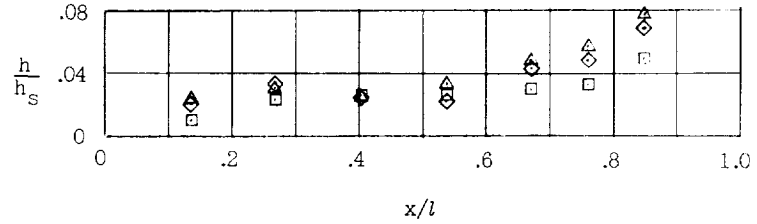

(b) $\alpha = 5^{\circ}$; sting 2.

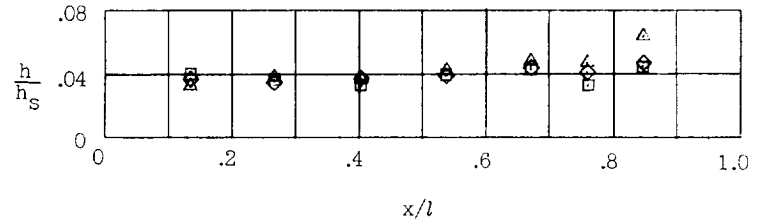

(c) $\alpha = 15^{\circ}$; sting 2.

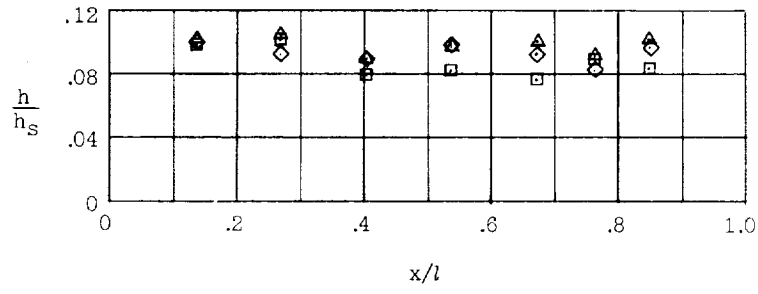

(d) $\alpha = 25^{\circ}$; sting 2.

	R_{∞}	h_s, $\frac{\text{Btu}}{(\text{ft}^2)(\text{sec})(^{\circ}\text{R})}$
○	0.10×10^6	0.210×10^{-2}
□	0.18×10^6	0.374×10^{-2}
◇	0.46×10^6	0.667×10^{-2}
△	1.36×10^6	1.180×10^{-2}

Figure 11.- Heat-transfer distribution along windward ray of afterbody.

[redacted]

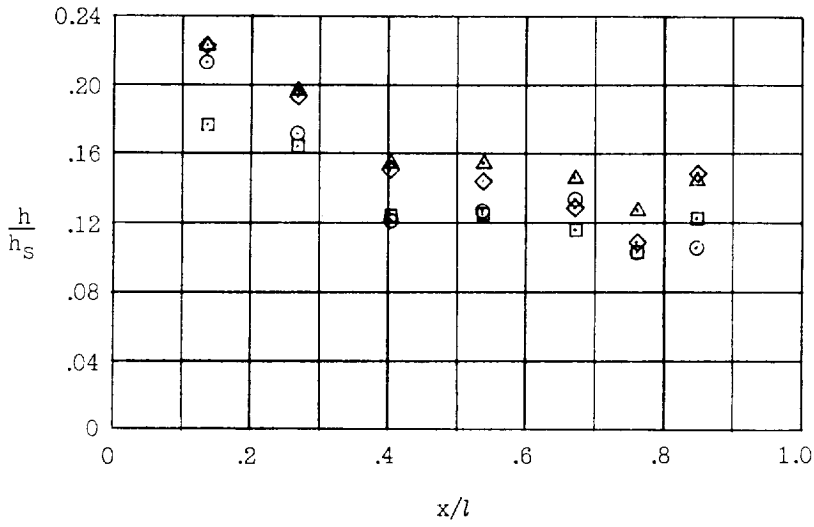

(e) $\alpha = 35^{\circ}$; sting 2.

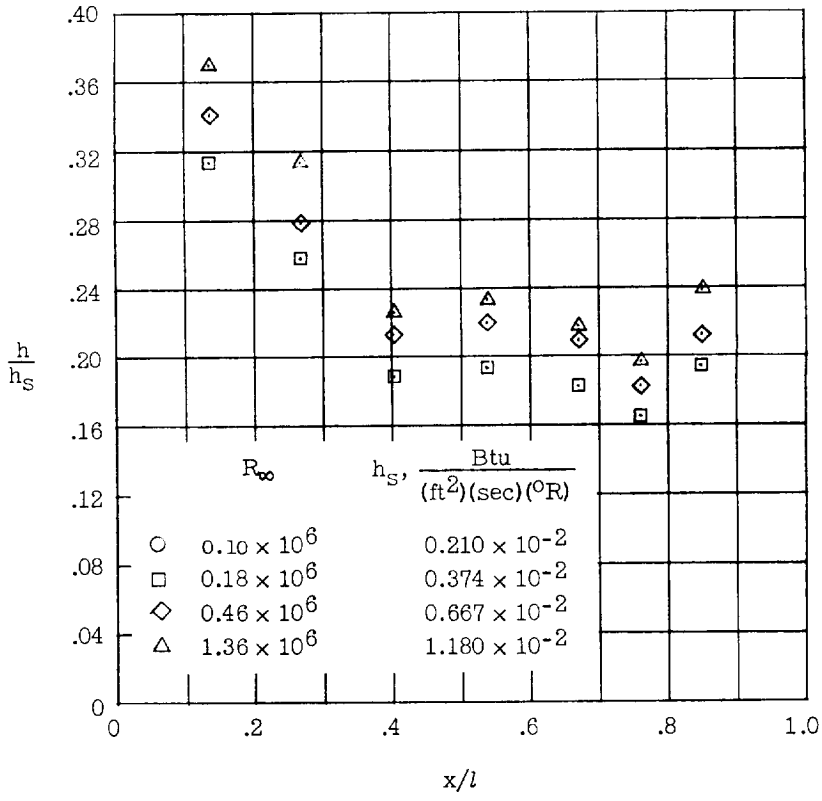

(f) $\alpha = 45^{\circ}$; sting 1.

Figure 11.- Continued.

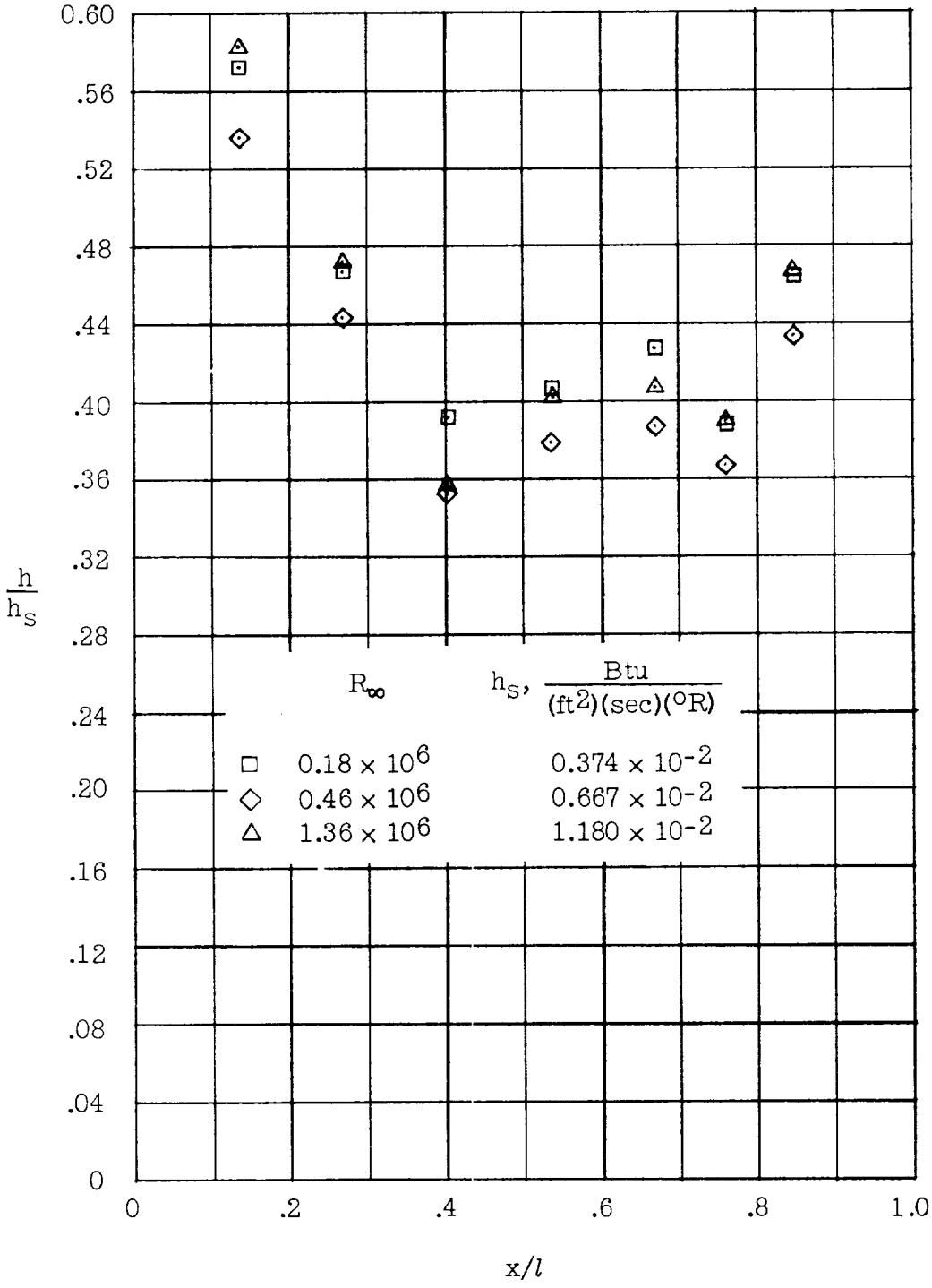

(g) $\alpha = 55^{\circ}$; sting 1.

Figure 11.- Concluded.

[redacted]

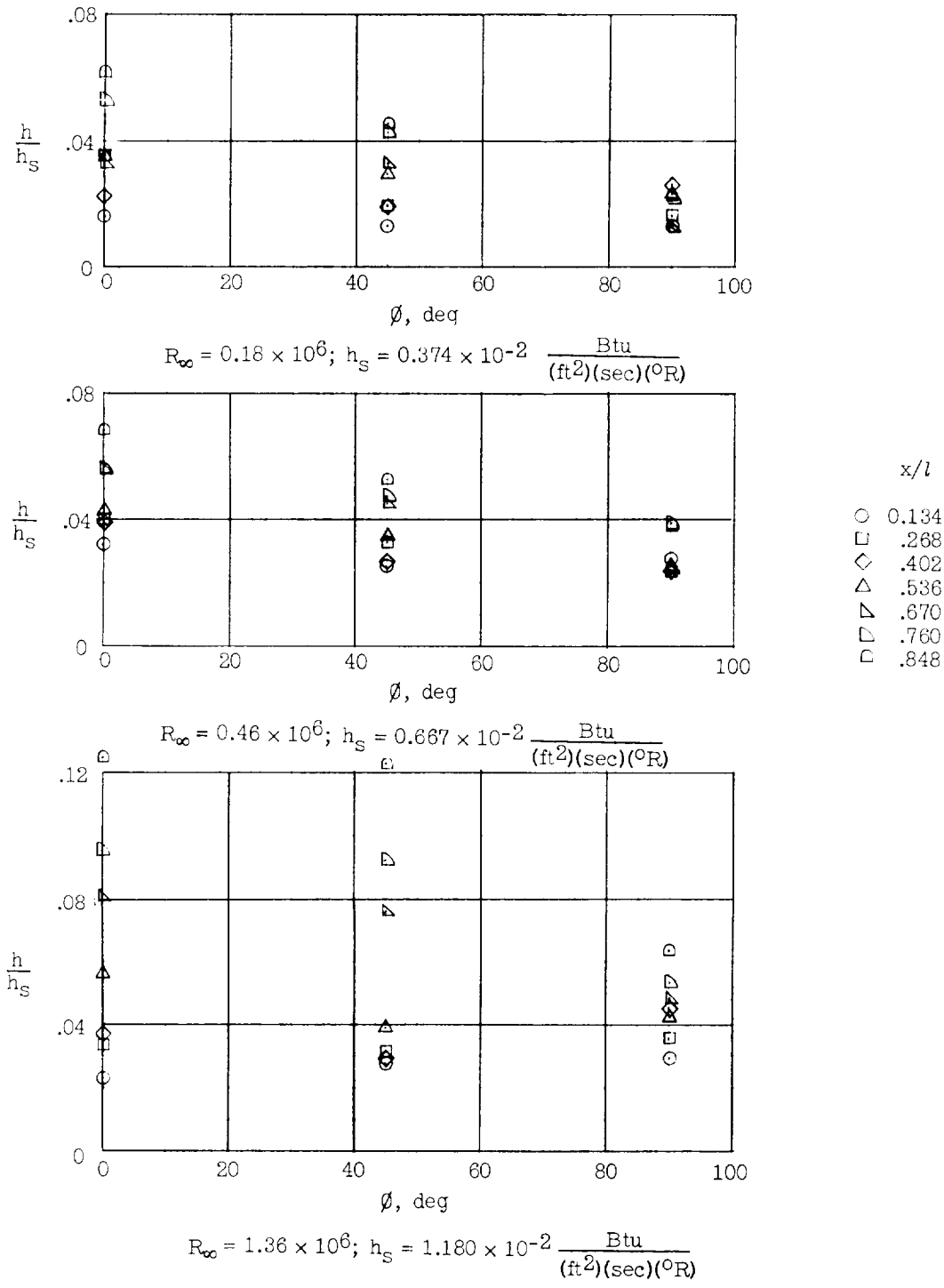

(a) Sting 2.

Figure 12.- Variation of heat transfer with angular location around afterbody at zero angle of attack.

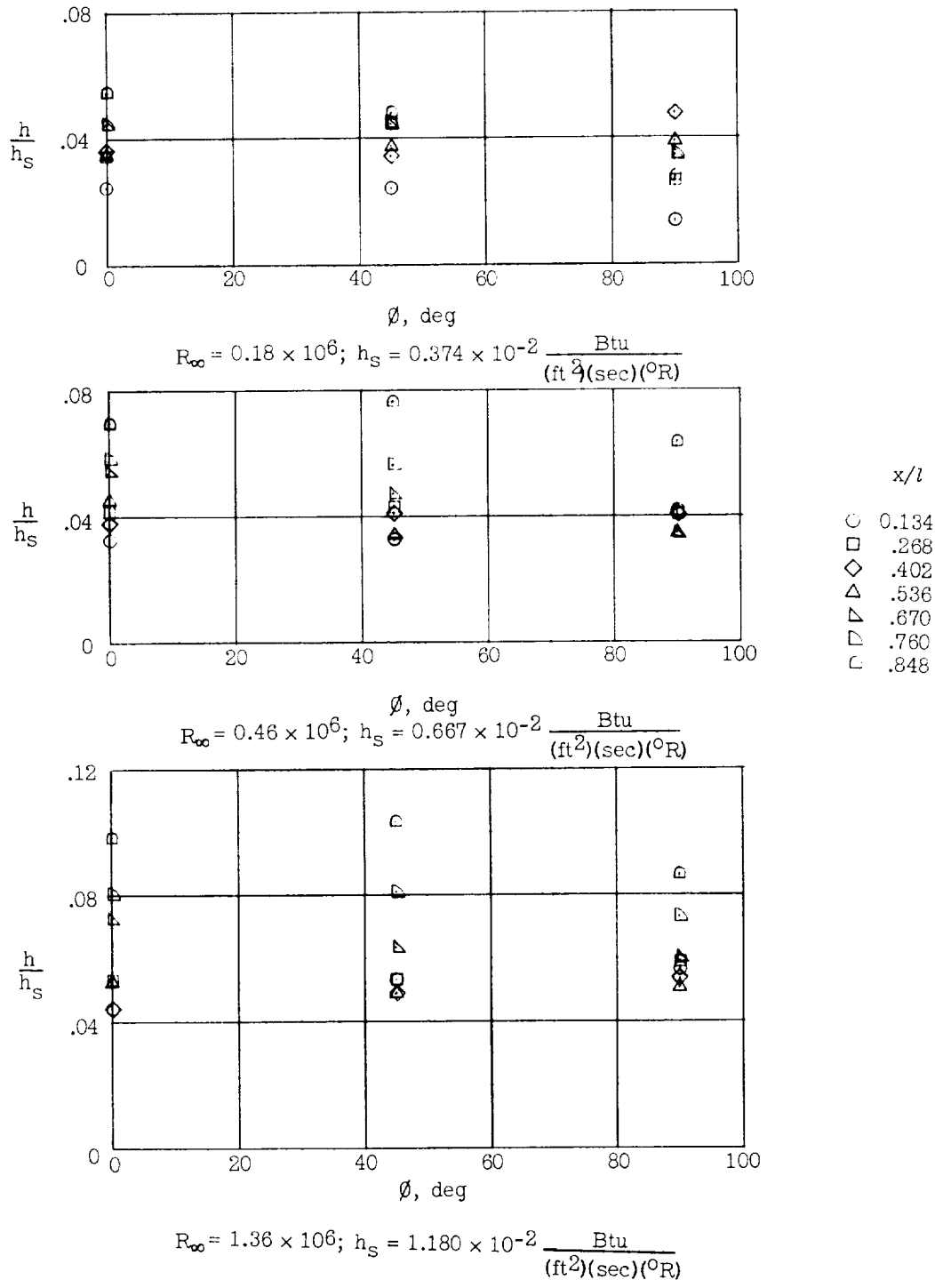

$R_\infty = 0.18 \times 10^6$; $h_s = 0.374 \times 10^{-2}$ Btu/(ft^2)(sec)($^\circ$R)

$R_\infty = 0.46 \times 10^6$; $h_s = 0.667 \times 10^{-2}$ Btu/(ft^2)(sec)($^\circ$R)

$R_\infty = 1.36 \times 10^6$; $h_s = 1.180 \times 10^{-2}$ Btu/(ft^2)(sec)($^\circ$R)

(b) Sting 3.

Figure 12.- Continued.

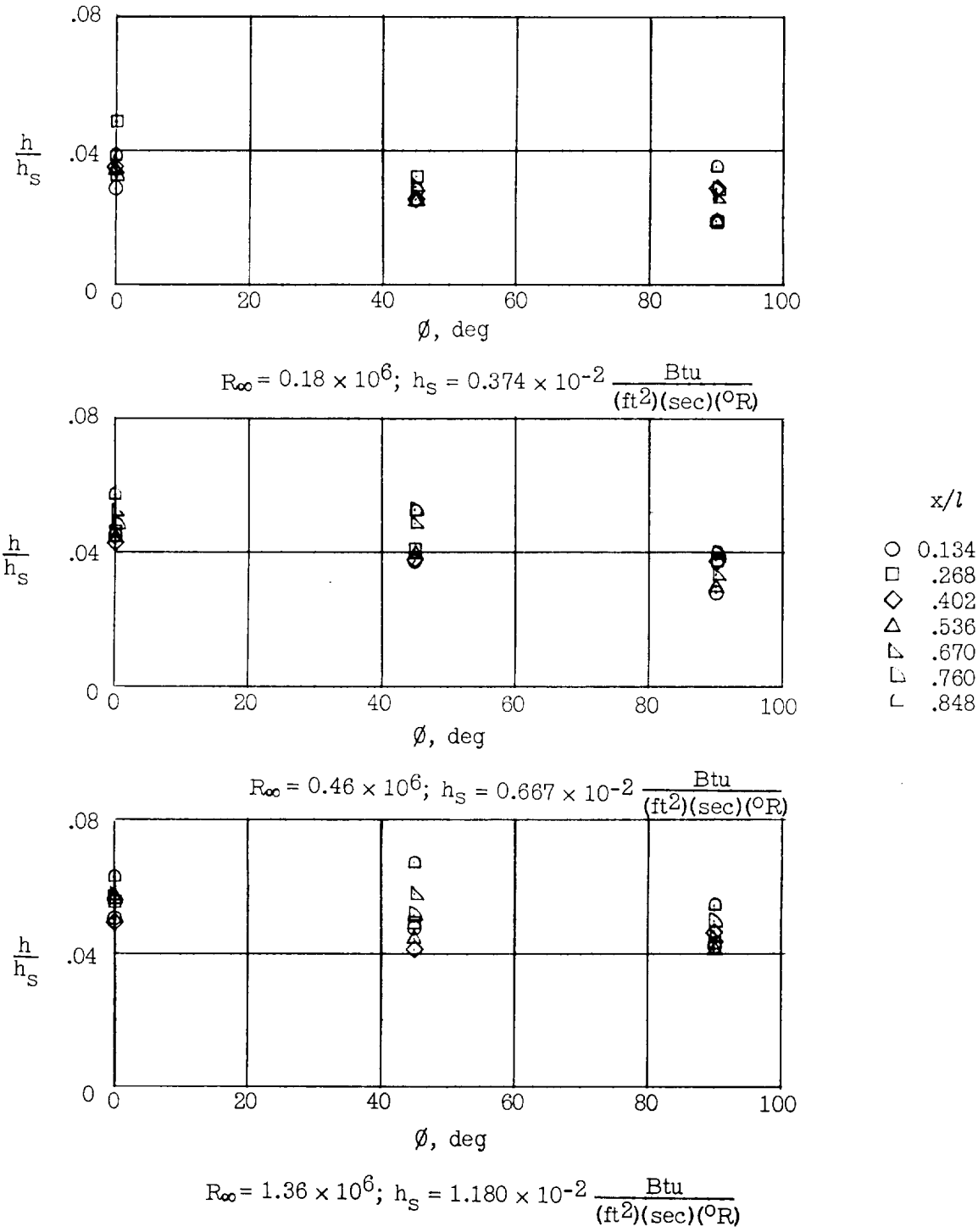

(c) Sting 3; 0.0075-inch roughness on face.

Figure 12.- Continued.

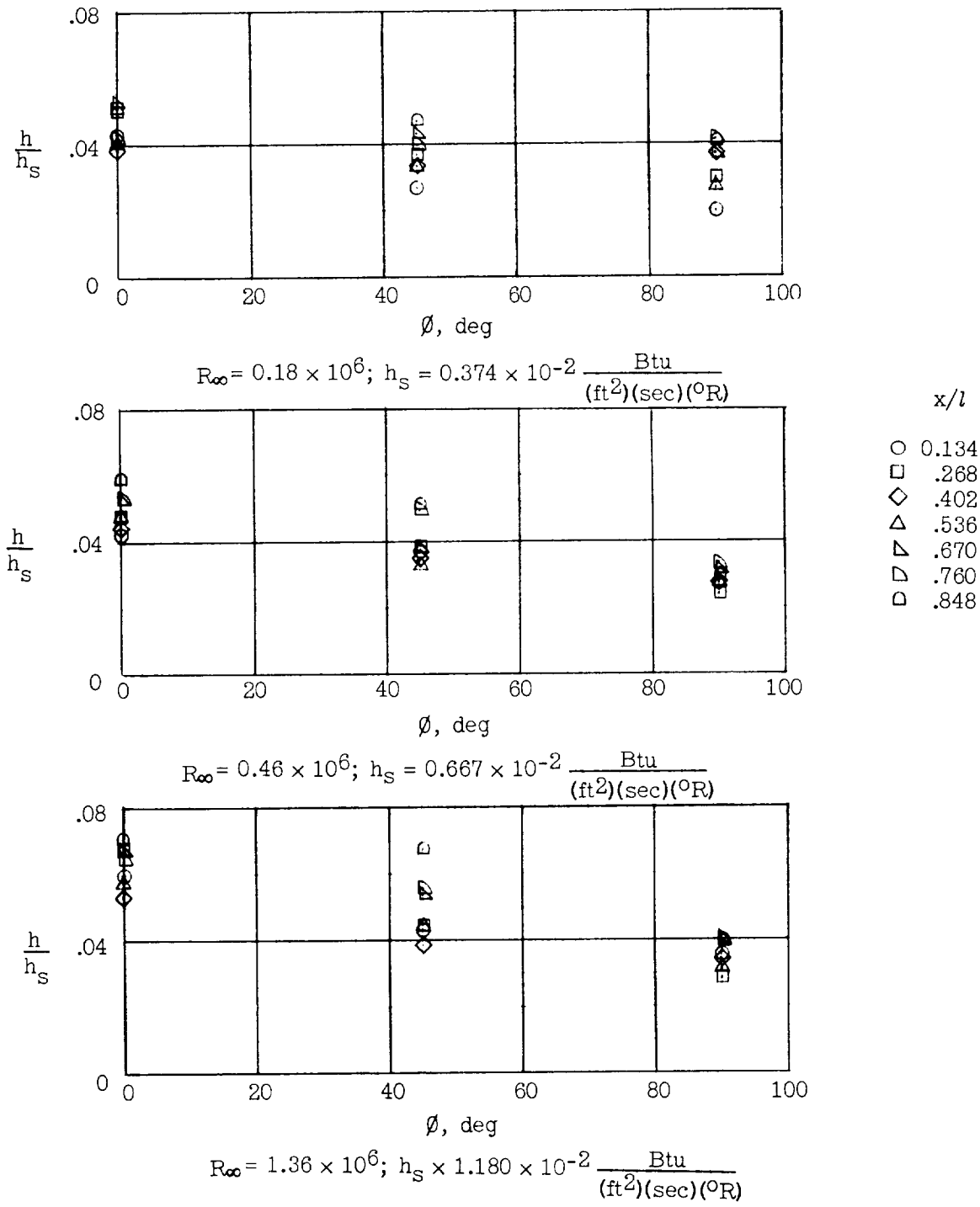

(d) Sting 3; 1/8-inch plate on each side of sting (70-percent increase in thickness).

Figure 12.- Concluded.

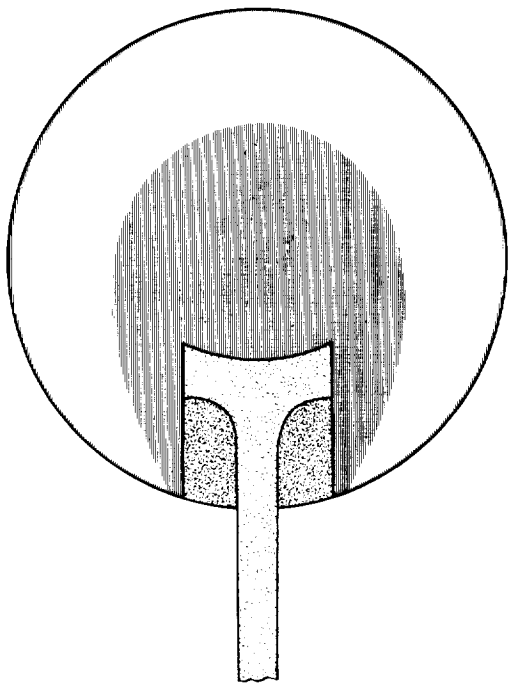

Sting 2 - Rear view

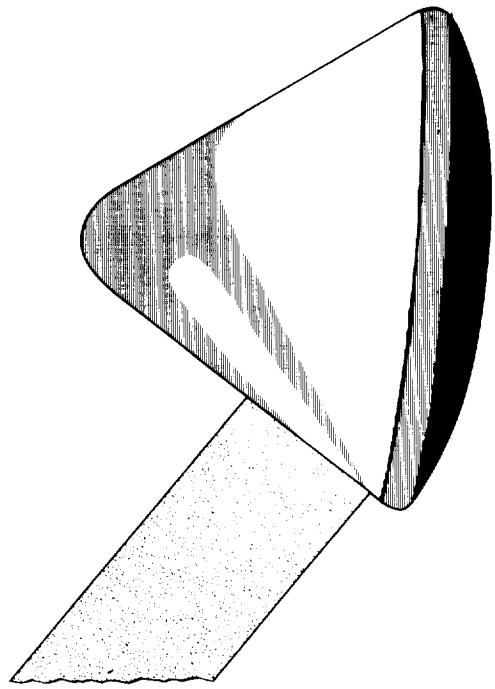

Sting 2 - Side view

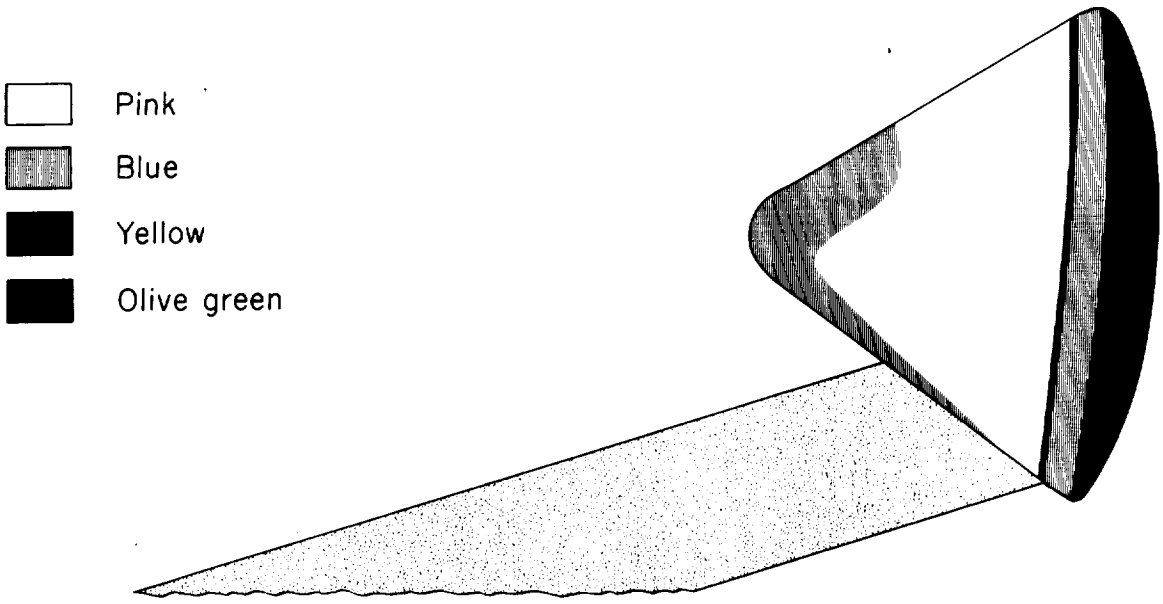

Sting 3 - Side view

Figure 13.- Sketch of temperature-sensitive-paint patterns at $\alpha = 0^{\circ}$.

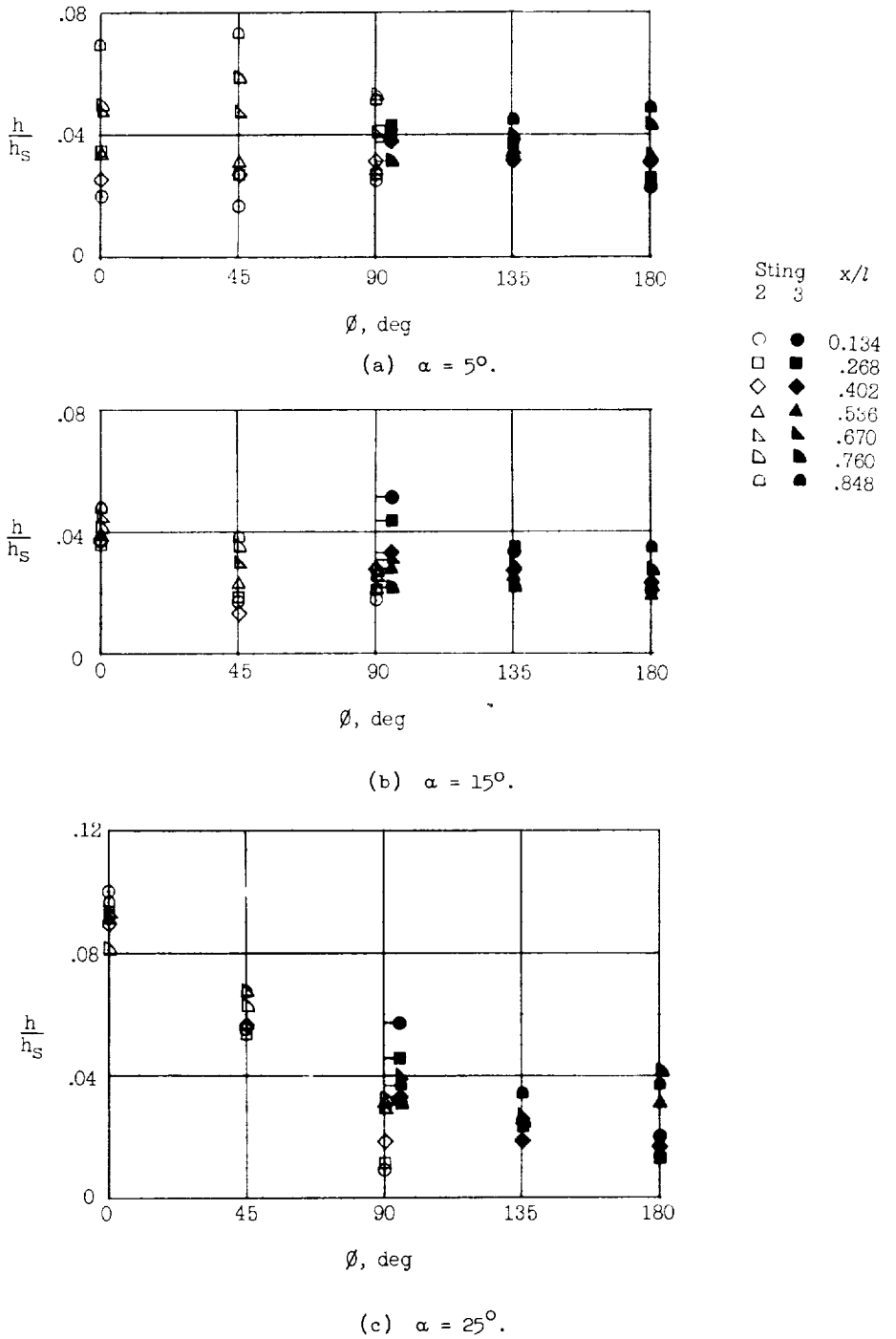

Figure 14.- Heat-transfer distribution around the afterbody at $\alpha = 5^\circ$ to 25°. $R_\infty = 0.46 \times 10^6$; $h_s = 0.667 \times 10^{-2}$ Btu/(ft^2)(sec)($^\circ$R).

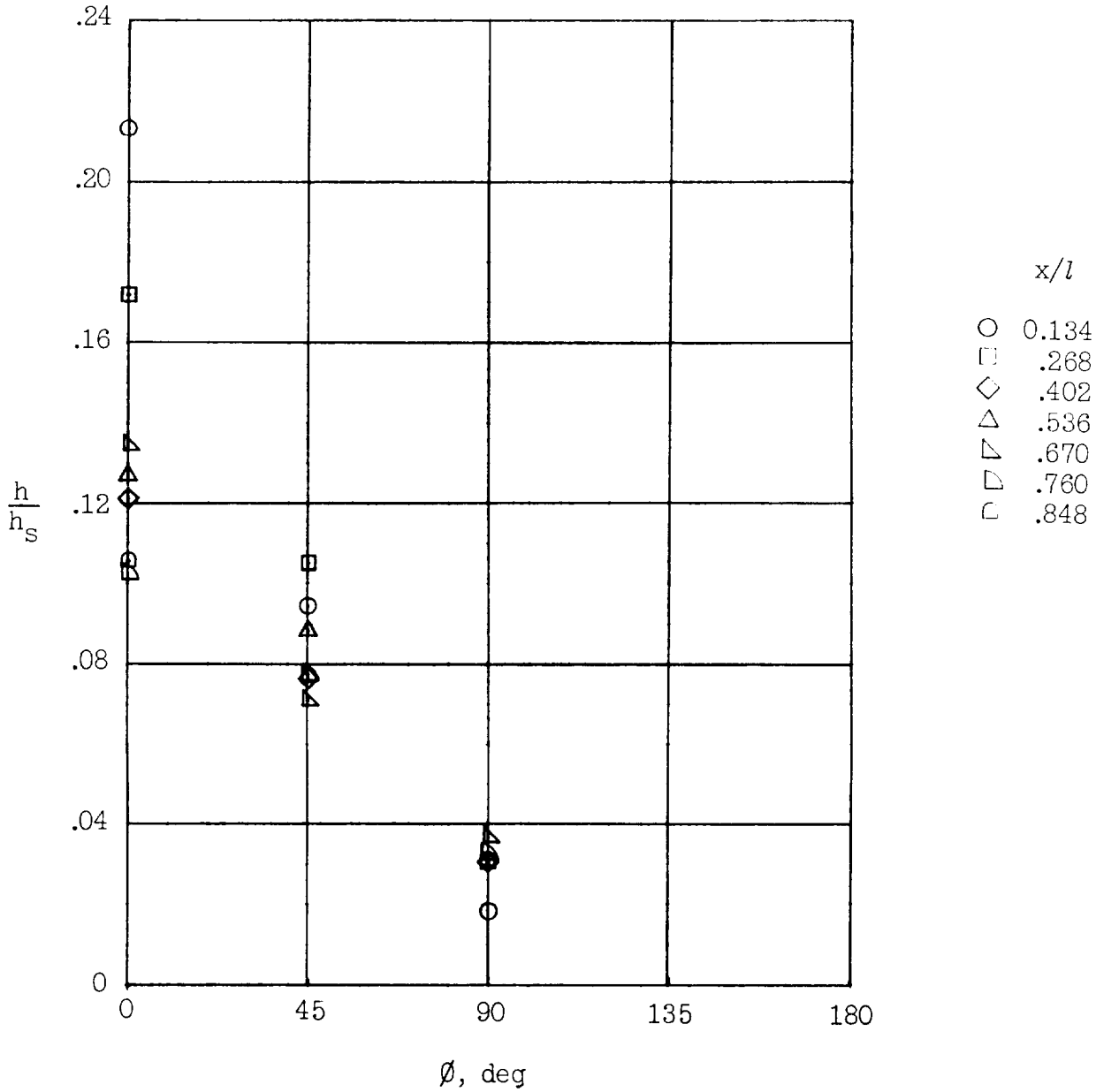

(a) $R_\infty = 0.10 \times 10^6$; $h_s = 0.210 \times 10^{-2}$ Btu/(ft^2)(sec)($^\circ$R); sting 1.

Figure 15.- Heat-transfer distribution around the afterbody at $\alpha = 35^\circ$.

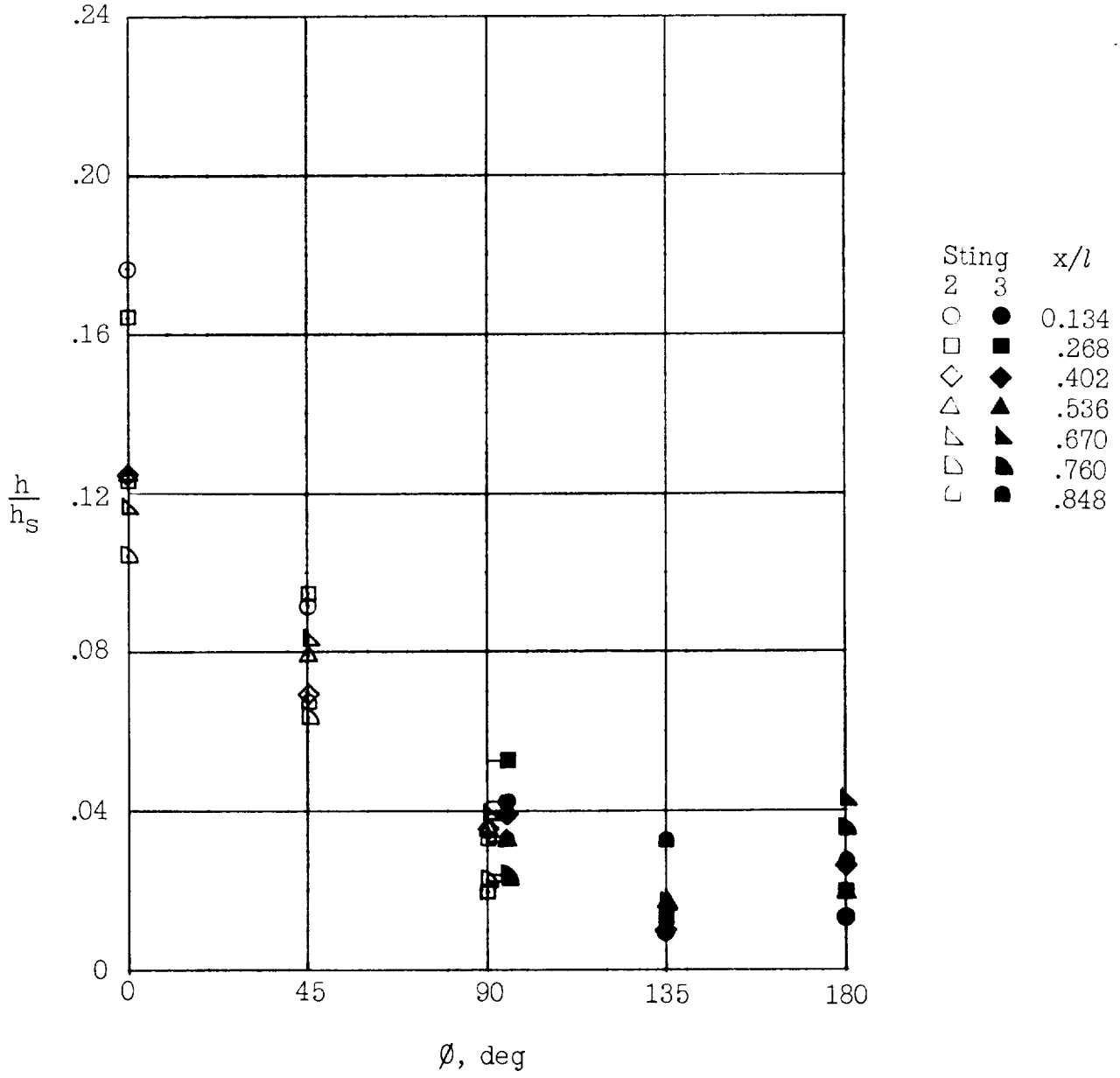

(b) $R_\infty = 0.18 \times 10^6$; $h_s = 0.374 \times 10^{-2}$ Btu/(ft^2)(sec)($^\circ$R).

Figure 15.- Continued.

[redacted]

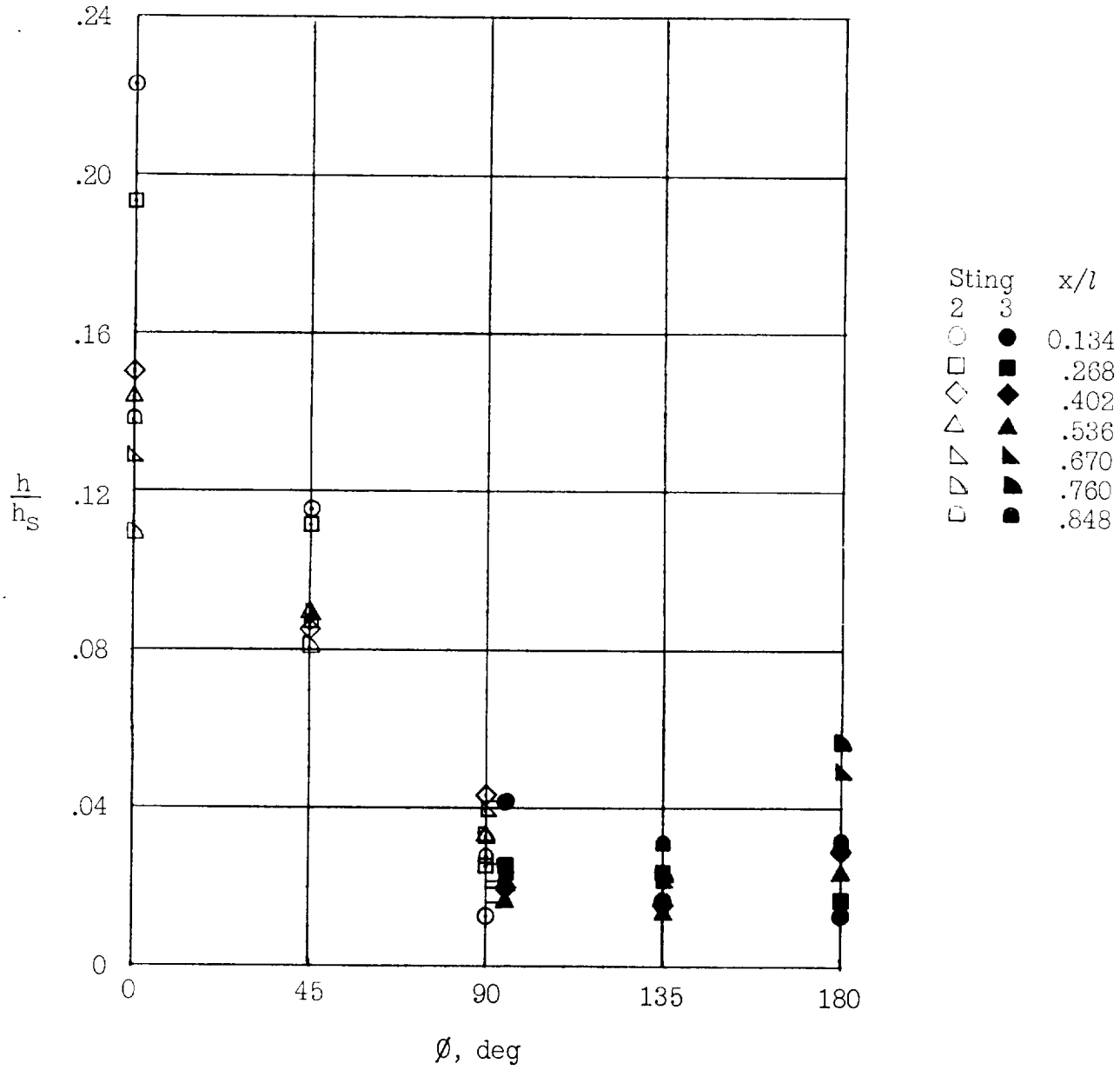

(c) $R_\infty = 0.46 \times 10^6$; $h_s = 0.667 \times 10^{-2}$ Btu/(ft^2)(sec)($^\circ$R).

Figure 15.- Continued.

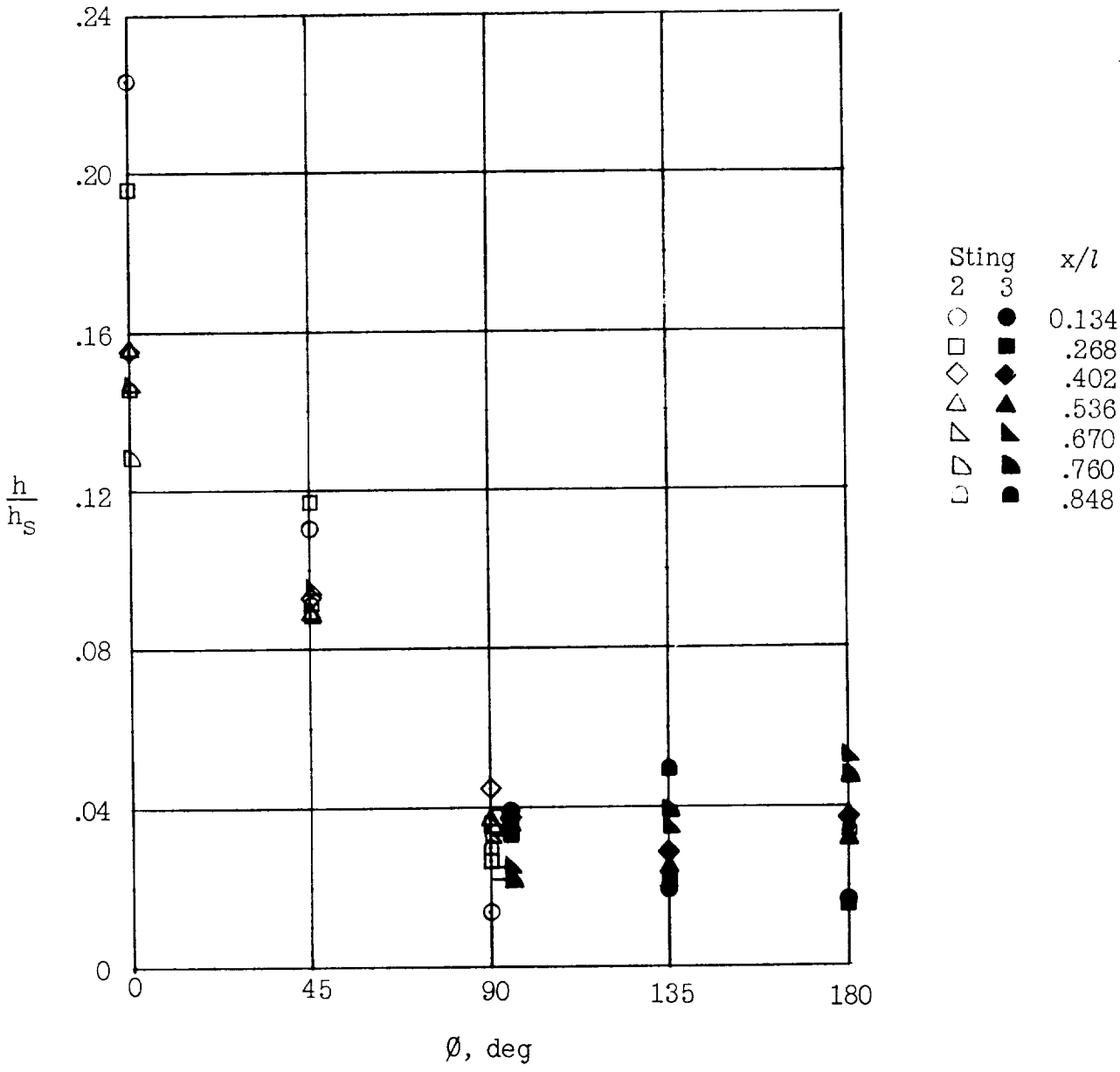

(d) $R_\infty = 1.36 \times 10^6$; $h_s = 1.180 \times 10^{-2}$ Btu/(ft^2)(sec)(°R).

Figure 15.- Concluded.

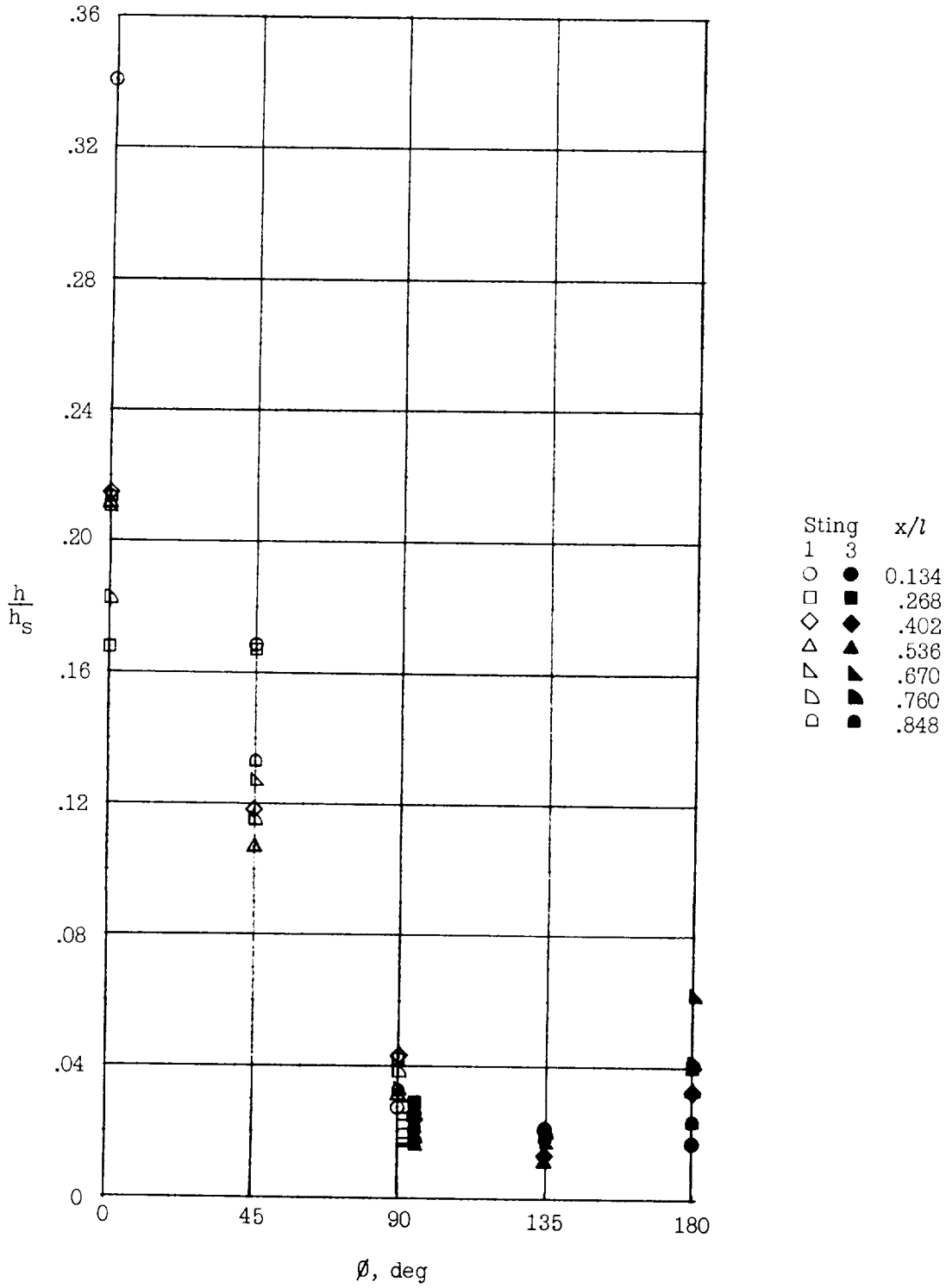

Figure 16.- Heat-transfer distribution around the afterbody at $\alpha = 45^{\circ}$. $R_{\infty} = 0.46 \times 10^{6}$; $h_s = 0.667 \times 10^{-2}$ Btu/(ft^2)(sec)($^{\circ}$R).

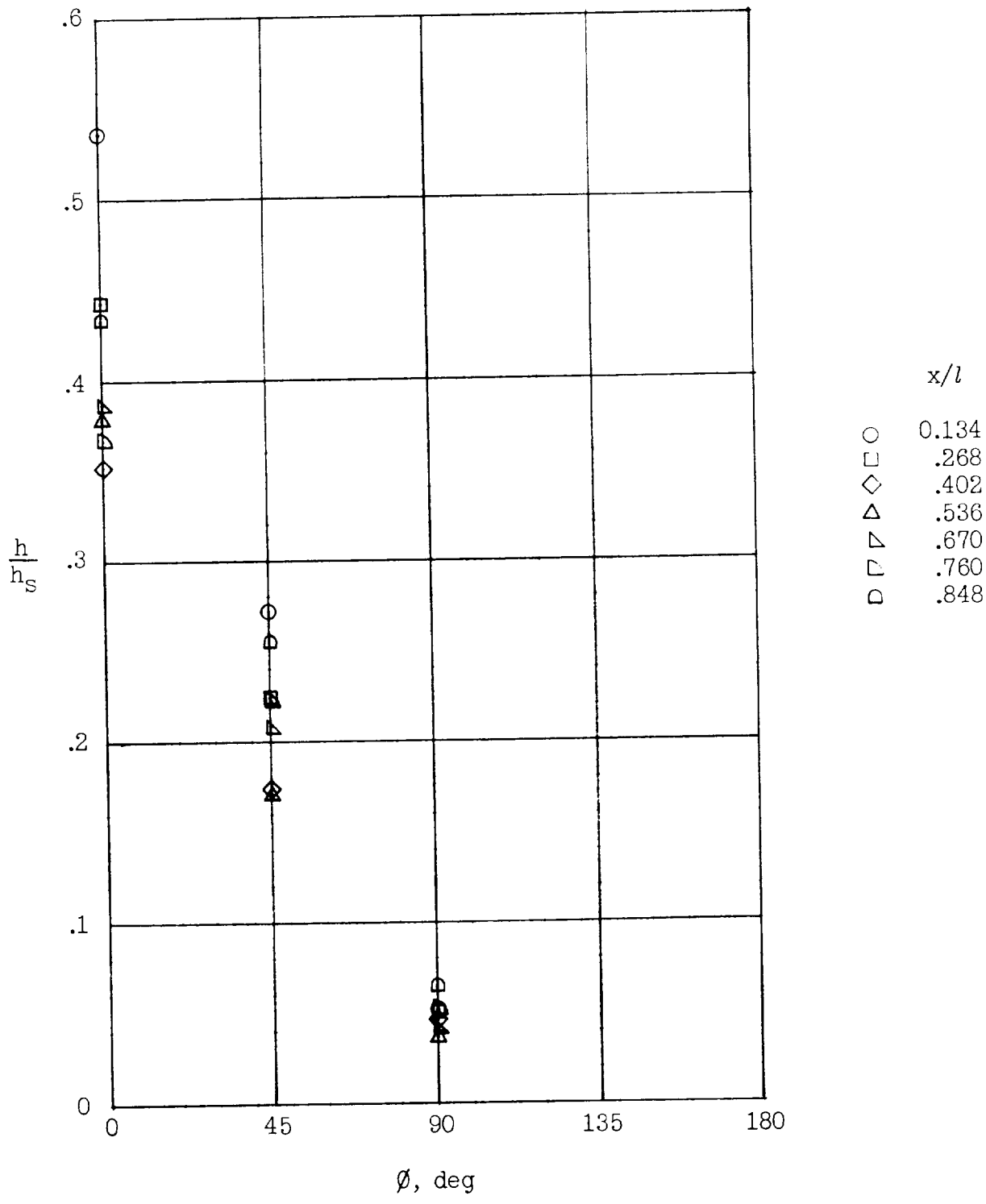

Figure 17.- Heat-transfer distribution around the afterbody at $\alpha = 55^{\circ}$. $R_{\infty} = 0.46 \times 10^{6}$; $h_s = 0.667 \times 10^{-2}$ Btu/(ft^2)(sec)($^{\circ}$R); sting 1.

NASA TM X-813 THIS CARD UNCLASSIFIED
National Aeronautics and Space Administration.
EXPERIMENTAL INVESTIGATION OF THE OVER-ALL PRESSURE DISTRIBUTION, FLOW FIELD, AND AFTERBODY HEAT-TRANSFER DISTRIBUTION OF AN APOLLO REENTRY CONFIGURATION AT A MACH NUMBER OF 8. Robert A. Jones. June 1963. 48p. (NASA TECHNICAL MEMORANDUM X-813. Supersedes NASA TM X-699)
([redacted]

Measured heat-transfer and [redacted]ributions on the afterbody of an Apollo configuration, the pressure distribution along the vertical plane of symmetry of the face, schlieren studies, oil-flow patterns, and wake surveys were obtained in a conventional Mach number 8 tunnel. The angle of attack was varied from 0° to 55°. The Reynolds number based on face diameter and free-stream properties ranged from 0.10×10^{6} to 1.36×10^{6}.

I. Jones, Robert A.
II. NASA TM X-813
III. NASA TM X-699

GROUP 4
Downgraded at 3 year intervals; declassified after 12 years

THIS CARD UNCLASSIFIED

NASA

NASA TM X-813 THIS CARD UNCLASSIFIED
National Aeronautics and Space Administration.
EXPERIMENTAL INVESTIGATION OF THE OVER-ALL PRESSURE DISTRIBUTION, FLOW FIELD, AND AFTERBODY HEAT-TRANSFER DISTRIBUTION OF AN APOLLO REENTRY CONFIGURATION AT A MACH NUMBER OF 8. Robert A. Jones. June 1963. 48p. (NASA TECHNICAL MEMORANDUM X-813. Supersedes NASA TM X-699)
[redacted]

Measured heat-transfer and pressure distributions on the afterbody of an Apollo configuration, the pressure distribution along the vertical plane of symmetry of the face, schlieren studies, oil-flow patterns, and wake surveys were obtained in a conventional Mach number 8 tunnel. The angle of attack was varied from 0° to 55°. The Reynolds number based on face diameter and free-stream properties ranged from 0.10×10^{6} to 1.36×10^{6}.

I. Jones, Robert A.
II. NASA TM X-813
III. NASA TM X-699

GROUP 4
Downgraded at 3 year intervals; declassified after 12 years

THIS CARD UNCLASSIFIED

NASA

NASA TM X-813 THIS CARD UNCLASSIFIED
National Aeronautics and Space Administration.
EXPERIMENTAL INVESTIGATION OF THE OVER-ALL PRESSURE DISTRIBUTION, FLOW FIELD, AND AFTERBODY HEAT-TRANSFER DISTRIBUTION OF AN APOLLO REENTRY CONFIGURATION AT A MACH NUMBER OF 8. Robert A. Jones. June 1963. 48p. (NASA TECHNICAL MEMORANDUM X-813. Supersedes NASA TM X-699)
([redacted]

Measured heat-transfer and pressure distributions on the afterbody of an Apollo configuration, the pressure distribution along the vertical plane of symmetry of the face, schlieren studies, oil-flow patterns, and wake surveys were obtained in a conventional Mach number 8 tunnel. The angle of attack was varied from 0° to 55°. The Reynolds number based on face diameter and free-stream properties ranged from 0.10×10^{6} to 1.36×10^{6}.

I. Jones, Robert A.
II. NASA TM X-813
III. NASA TM X-699

GROUP 4
Downgraded at 3 year intervals; declassified after 12 years

THIS CARD UNCLASSIFIED

NASA

NASA TM X-813 THIS CARD UNCLASSIFIED
National Aeronautics and Space Administration.
EXPERIMENTAL INVESTIGATION OF THE OVER-ALL PRESSURE DISTRIBUTION, FLOW FIELD, AND AFTERBODY HEAT-TRANSFER DISTRIBUTION OF AN APOLLO REENTRY CONFIGURATION AT A MACH NUMBER OF 8. Robert A. Jones. June 1963. 48p. (NASA TECHNICAL MEMORANDUM X-813. Supersedes NASA TM X-699)
[redacted]

Measured heat-transfer and pressure distributions on the afterbody of an Apollo configuration, the pressure distribution along the vertical plane of symmetry of the face, schlieren studies, oil-flow patterns, and wake surveys were obtained in a conventional Mach number 8 tunnel. The angle of attack was varied from 0° to 55°. The Reynolds number based on face diameter and free-stream properties ranged from 0.10×10^{6} to 1.36×10^{6}.

I. Jones, Robert A.
II. NASA TM X-813
III. NASA TM X-699

GROUP 4
Downgraded at 3 year intervals; declassified after 12 years

THIS CARD UNCLASSIFIED

NASA

NASA TM X-813 THIS CARD UNCLASSIFIED
National Aeronautics and Space Administration.
EXPERIMENTAL INVESTIGATION OF THE OVER-ALL PRESSURE DISTRIBUTION, FLOW FIELD, AND AFTERBODY HEAT-TRANSFER DISTRIBUTION OF AN APOLLO REENTRY CONFIGURATION AT A MACH NUMBER OF 8. Robert A. Jones. June 1963. 48p. (NASA TECHNICAL MEMORANDUM X-813. Supersedes NASA TM X-699)
([redacted]

Measured heat-transfer and pressure distributions on the afterbody of an Apollo configuration, the pressure distribution along the vertical plane of symmetry of the face, schlieren studies, oil-flow patterns, and wake surveys were obtained in a conventional Mach number 8 tunnel. The angle of attack was varied from 0° to 55°. The Reynolds number based on face diameter and free-stream properties ranged from 0.10×10^{6} to 1.36×10^{6}.

I. Jones, Robert A.
II. NASA TM X-813
III. NASA TM X-699

GROUP 4
Downgraded at 3 year intervals; declassified after 12 years

THIS CARD UNCLASSIFIED

NASA

NASA TM X-813 THIS CARD UNCLASSIFIED
National Aeronautics and Space Administration.
EXPERIMENTAL INVESTIGATION OF THE OVER-ALL PRESSURE DISTRIBUTION, FLOW FIELD, AND AFTERBODY HEAT-TRANSFER DISTRIBUTION OF AN APOLLO REENTRY CONFIGURATION AT A MACH NUMBER OF 8. Robert A. Jones. June 1963. 48p. (NASA TECHNICAL MEMORANDUM X-813. Supersedes NASA TM X-699)
[redacted]

Measured heat-transfer and pressure distributions on the afterbody of an Apollo configuration, the pressure distribution along the vertical plane of symmetry of the face, schlieren studies, oil-flow patterns, and wake surveys were obtained in a conventional Mach number 8 tunnel. The angle of attack was varied from 0° to 55°. The Reynolds number based on face diameter and free-stream properties ranged from 0.10×10^{6} to 1.36×10^{6}.

I. Jones, Robert A.
II. NASA TM X-813
III. NASA TM X-699

GROUP 4
Downgraded at 3 year intervals; declassified after 12 years

THIS CARD UNCLASSIFIED

NASA

NASA TM X-813 THIS CARD UNCLASSIFIED
National Aeronautics and Space Administration.
EXPERIMENTAL INVESTIGATION OF THE OVER-ALL PRESSURE DISTRIBUTION, FLOW FIELD, AND AFTERBODY HEAT-TRANSFER DISTRIBUTION OF AN APOLLO REENTRY CONFIGURATION AT A MACH NUMBER OF 8. Robert A. Jones. June 1963. 48p. (NASA TECHNICAL MEMORANDUM X-813. Supersedes NASA TM X-699)
([redacted]

Measured heat-transfer and pressure distributions on the afterbody of an Apollo configuration, the pressure distribution along the vertical plane of symmetry of the face, schlieren studies, oil-flow patterns, and wake surveys were obtained in a conventional Mach number 8 tunnel. The angle of attack was varied from 0° to 55°. The Reynolds number based on face diameter and free-stream properties ranged from 0.10×10^{6} to 1.36×10^{6}.

I. Jones, Robert A.
II. NASA TM X-813
III. NASA TM X-699

GROUP 4
Downgraded at 3 year intervals; declassified after 12 years

THIS CARD UNCLASSIFIED

NASA

NASA TM X-813 THIS CARD UNCLASSIFIED
National Aeronautics and Space Administration.
EXPERIMENTAL INVESTIGATION OF THE OVER-ALL PRESSURE DISTRIBUTION, FLOW FIELD, AND AFTERBODY HEAT-TRANSFER DISTRIBUTION OF AN APOLLO REENTRY CONFIGURATION AT A MACH NUMBER OF 8. Robert A. Jones. June 1963. 48p. (NASA TECHNICAL MEMORANDUM X-813. Supersedes NASA TM X-699)
([redacted]

Measured heat-transfer and pressure distributions on the afterbody of an Apollo configuration, the pressure distribution along the vertical plane of symmetry of the face, schlieren studies, oil-flow patterns, and wake surveys were obtained in a conventional Mach number 8 tunnel. The angle of attack was varied from 0° to 55°. The Reynolds number based on face diameter and free-stream properties ranged from 0.10×10^{6} to 1.36×10^{6}.

I. Jones, Robert A.
II. NASA TM X-813
III. NASA TM X-699

GROUP 4
Downgraded at 3 year intervals; declassified after 12 years

THIS CARD UNCLASSIFIED

NASA